Hydrothermal quartz-baryte veins containing Pb-Cu-Sb-(Bi) mineralization at Brusno-Brzáčka occurrence (Veporic Unit, Central Slovakia) and their supergene alteration

Eva Hoppanová[1*], Štefan Ferenc[1], Tomáš Mikuš[2], Zdeněk Dolníček[3], Richard Kopáčik[1], Jozef Vlasáč[2], Viera Šimonová[1]

[1] Department of Geography and Geology, Faculty of Natural Sciences, Matej Bel University, Tajovského 40, 974 01 Banská Bystrica, Slovakia; *e-mail: ehoppanova@umb.sk
[2] Earth Science Institute of the Slovak Academy of Sciences, Ďumbierska 1, 974 11 Banská Bystrica, Slovakia
[3] Department of Mineralogy and Petrology, National Museum,Cirkusová 1740, 193 00 Praha 9-Horní Počernice, Czech Republic

AGEOS

Abstract: The Brzáčka occurrence (N 48.7698772°; E 19.4128150°) is located near the Brusno village (Slovenské Rudohorie Mts. Veporic Unit). Historically, the mineralization was explored by small-scale mining works located at the contact between the siliciclastic rocks of the Upper Permian and the Lower Triassic age. Paleo-Alpine metamorphic-hydrothermal mineralization is represented by quartz, baryte, or quartz-baryte veins, containing weak ore mineralization. Its succession is as follows: coarse-grained quartz I, pyrite (mineralization period I); baryte (II); tetrahedrite-(Zn), chalcopyrite (III); galena (IV) and quartz II (V). Supergene alteration produced initially covellite and spionkopite in the cementation zone. The oldest minerals in the oxidation zone are goethite, pyromorphite and mimetite. They were succeeded by the crystallization of Ba-rich anglesite, which partly overlaps in time with the precipitation of slightly younger anglesite. The formation of baryte partly overlaps with the deposition of anglesite, but in most cases, it is clearly younger. Bismutite is the youngest supergene mineral. A solid solution of anglesite – baryte with a Ba content from 0.29 *apfu* up to 0.51 *apfu* (i.e., Ba-rich anglesite) was identified at the studied site. This mineral phase covers the field of immiscibility of the natural solid solution $PbSO_4$ – $BaSO_4$, but the Ba/Pb ratio practically does not enter to the baryte field (Pb-rich baryte).

Key words: sulfide mineralization, quartz-baryte vein, supergene alteration, baryte-anglesite solid solution, Veporic Unit, Slovenské Rudohorie Mts., Western Carpathians

1. INTRODUCTION

There is a number of small historic deposits and mineralogical occurrences of Fe, Cu, Ag and Sb ores in the northern part of the Veporic Superunit of the Western Carpathians. The most important ones are located around the villages of Špania Dolina, Staré Hory, Poniky, Ľubietová and Čierny Balog. Less known occurrences of Cu, Fe, Pb, Zn, Ag, As, Au mineralization were also found near the villages Šumiac, Bacúch, Beňuš, Pohronská Polhora, Polomka, or Harmanec (Slavkay & Petro, 1993; Slavkay et al., 2004).

One of these occurrences is represented by the hydrothermal quartz-baryte veins with poor Pb-Cu-Sb-(Bi) mineralization at the Brzáčka locality, south of the Brusno village. The data on this occurrence are very austere (Hvožďara, 1971, 1980). The presented contribution expands basic knowledge about the nature of primary mineralization at this locality, and it is also dedicated to the mineralogical characteristics of its supergene transformation.

2. GEOLOGICAL SETTING OF WIDER AREA

The Western Carpathians Mts. located in the Central Europe are a part of the Alpine-Himalayan Mountain range. Today's geological structure of the Western Carpathians is the result of complex geotectonic events during the Hercynian and Alpine orogeny. The Western Carpathians are divided into two basic units, from the point of view of rock filling, the age of the tectonic individualization of the units and their mutual relations: externides and internides. The internides are built by a system of the superficial nappes – Fatric, Hronic and Silicic (without crystalline complexes), and the fundamental nappes (main tectonic superunits with crystalline complexes) – Tatric, Veporic and Gemeric. Those are thrusted onto each other in the general direction from the S to N (Tatric is the structurally lowest and northernmost unit), in frame of the Alpine Orogeny style (Maheľ et al., 1967; Mazúr & Lukniš, 1980, 1986; Putiš, 1992; Plašienka et al., 1997; Plašienka, 1999; Hók et al., 2019; Kováč & Plašienka, 2003). The geological setting of the Veporic Unit is mainly formed by a crystalline basement of Palaeozoic age and the autochthonous cover of the Upper Palaeozoic (Upper Permian) to Mesozoic (Lower Cretaceous) stratigraphic range (Siegel, 1982; Vozárová & Vozár, 1988; Hók et al., 2019; Slavkay et al., 2004; Antalík & Káčer, 2005).

The area of interest lies in the wider region of the Ľubietová zone – Veľký Bok Unit of the Veporic Unit (Zoubek, 1936, 1957); and particularly in the Upper Palaeozoic rocks of a Northern Veporic cover (Vozárová, 1979). The Ľubietová

Manuscript received 2023-12-5
Revised version accepted 2023-02-23

zone is built up by three, NE-SW oriented segments differring in their lithology (Slavkay et al., 2004; Lexa et al., 2007). It lithologically consists of various rocks: orthogneisses to migmatites with bodies of amphibolites, leucocratic granitoids and paragnisses.

The sedimentary cover of the Northern Veporic crystalline is formed by Permian sequences of the Ľubietová Group (Slavkay et al., 2004). Vozárová (1979) recognized two lithostratigraphic units here - the lower Brusno and the upper Predajná formations. The rocks of both formations (originally continental coarse-clastic sediments of the "red-beds" type) were Alpine metamorphosed in the quartz-muscovite-chlorite subfacies of greenschist facies (Vozárová, l979). The Brusno Formation (Lower Permian) is built up of weakly metamorphosed conglomerates, arcoses, cherts and volcanics rocks. In the upper part, it is characterized by the presence of the volcanogenic horizon of Harnobis (rhyodacite and andesite tuff to ignimbrite, epiclastics and lava flows; Slavkay et al., 2004). The Predajná Formation (Upper Permian) is formed by complexes of varied sandstones, polymict conglomerates and sandy shales (Vozárová, 1979; Slavkay et al., 2004). The Permian age of the sediments of the Ľubietová Group is evidenced by the palynomorph community (Planderová & Vozárová, 1982) and SHRIMP dating of magmatic zircons from Harnobis volcanics, which yielded ages of 273±6 and 279±4 Ma (Vozárová et al., 2016).

3. LOCALIZATION, GEOLOGY AND MINERALOGY OF STUDIED OCCURRENCE

The studied occurrence Brusno-Brzáčka is located in the western part of the Slovenské Rudohorie Mts., in the Veporské vrchy Mts. (central Slovakia). The geological settings of the north-western part of the Slovenské Rudohorie Mts. were described by Polák et al. (2003[a, b]).

The Brzáčka occurrence is located about 3.6 km SSE of the Brusno village, 4.5 km NE of the Ľubietová village, approximately 750 m NW of the elevation of Brzáčka (1005 m a. s. l.), at an altitude of about 780 m. The geographical coordinates of the center of occurrence (the adit under the forest road) are N 48.7698772°; E 19.4128150°.

In the past, perhaps in the 19th century, mineralization was explored by small-scale mining works (an adit, an exploration trench and several shafts were realized here). The gallery directs 160° to the SSE. In addition, 9 shafts above the gallery and one short exploration trench in the direction of 132° to the SE can be still found here.

The old mining are located at the contact between the Upper Permian rocks (Ľubietová Group) and the Lower Triassic rocks of the Veľký Bok Unit (Hvožďara, 1971, 1980; Koděra et al., 1986; Fig. 1). The Permian is represented by metaconglomerates, metasandstones, sandy shales, metarhyolites – metadacites and their volcanoclastics. The Lower Triassic is built by quartz sandstones, quartzites, conglomerates, sporadically shales and siltstones. In the vicinity of the adit, the rocks are relatively intensively tectonized and altered to fine-grained white mica phyllites. Blocks of secretion quartz (size approximately 1 x 1 m) without ore mineralization are also found. The nature of primary mineralization can be assessed only on the basis of material from the adit dump and forest road cuts. The heaps of the exploration shafts are devoid of ore material (except for rare pyrite in the quartz gangue).

The mineralogy of the occurrence was studied in the past by Hvožďara (1971, 1980), who found here primary baryte, quartz, pyrite, chalcopyrite, galena and secondary goethite. In addition to these minerals, the results of the new revision of the site showed the presence of hematite and minerals of the tetrahedrite series (primary minerals). Supergene weathering products are represented by baryte, anglesite, bismutite, pyromorphite, mimetite, covellite and spionkopite.

4. METHODS

The ore samples for the mineralogical research were taken from the old adit dump and forest road cuts. The position of the individual mine works (adit, exploration trench and shafts) were targeted with a tourist GPS device with an accuracy of ±5 m.

Microscopic properties of mineral phases were observed in both transmitted and reflected light (polished thin sections) using a Nikon ECLIPSE LV 100 POL polarizing microscope (Matej Bel University, Banská Bystrica).

The chemical composition of minerals was quantitatively studied using an electron microanalyzer Jeol-JXA-8530F (Institute of Earth Sciences SAS, Banská Bystrica) and Cameca SX-100 (National Museum, Prague, Czech Republic). In addition to point wavelength-dispersive microanalyses (WDS), the microanalyzer was also used for the purposes of photo-documentation in backscattered electrons (BSE) and non-standardized energy-dipersive analyses (EDS). The WDS microanalyses were performed under the following conditions: acceleration voltage 20 and 25 kV, measurement current 15 and 20 nA and electron beam diameter 2–5 μm (sulphides) and 15 kV, measurement current 15 nA and 10nA and electron beam diameter 1–10 μm (supergene minerals). The electron microanalyzer (EMP) was calibrated using natural and synthetic standards (Supplementary table S1). The tables presented in the following text do not include elements whose content values were below the detection limit for individual elements (0.03–0.2 wt. %). The PAP (Pouchou & Pichoir 1985) and ZAF corrections were used.

4.1. Primary (hydrothermal) minerals

The dominant filling of hydrothermal veins is monomineral quartz or baryte, but also quartz and baryte. Sulfide minerals are disseminated, or rarely form nests (size to the first cm) in gangue. The main sulfide minerals are pyrite and rarely galena, accompanied by chalcopyrite and tetrahedrite-(Zn). However, the ore mineralization is poor and the occurrence has only character of an ore indication.

Pyrite is relatively abundant in small amounts. Its accumulations up to 2 cm in size were rarely found in the quartz gangue. Crushed anhedral pyrite grains and fine-grained clusters (up to

0.1 mm) are enclosed in tetrahedrite-(Zn), goethite and anglesite (Fig. 2a, b). More rarely, they are surrounded by fine-grained white mica. The chemical composition of pyrite (1 WDS analysis) shows slightly increased contents of Cu (0.01 *apfu*).

Chalcopyrite forms local nests (up to 3 cm in size), especially in quartz gangue. The microscopic description practically coincides with pyrite, but chalcopyrite is not cataclased. It is younger than pyrite. Non-standardized EDS analyses did not show the presence of other elements.

Galena forms 3–4 mm large aggregates in quartz. Under the microscope, its considerable supergene transformation is evident. It is characterized by a system of cleavage cracks in three directions, accompanied by triangular pits. Galena tends to be surrounded by anglesite, which also replaces it along cracks. There are also small nests of covellite and spionkopite in anglesite. Sometimes anglesite forms complete pseudomorphs after galena, preserving the cubic shape of the original mineral (Fig. 2c, d). The chemical composition of galena is quite interesting (considering mainly "pure" composition of other galenas in the Veporic Unit), but without significant variations in the elements content (Tab. 1). In addition to lead, Bi (average 0.02 *apfu*) and Ag (average 0.01 *apfu*) are present in the cationic position. Copper is less significant (up to 0.02 *apfu*). In addition to sulfur, a small amount of Se (up to 0.01 *apfu*) is present in the anionic position. The average empirical formula of galena from Brzáčka (7 WDS analyses) can be expressed as $(Pb_{0.97}Bi_{0.02}Ag_{0.01})_{\Sigma 1.00}S_{0.99}$.

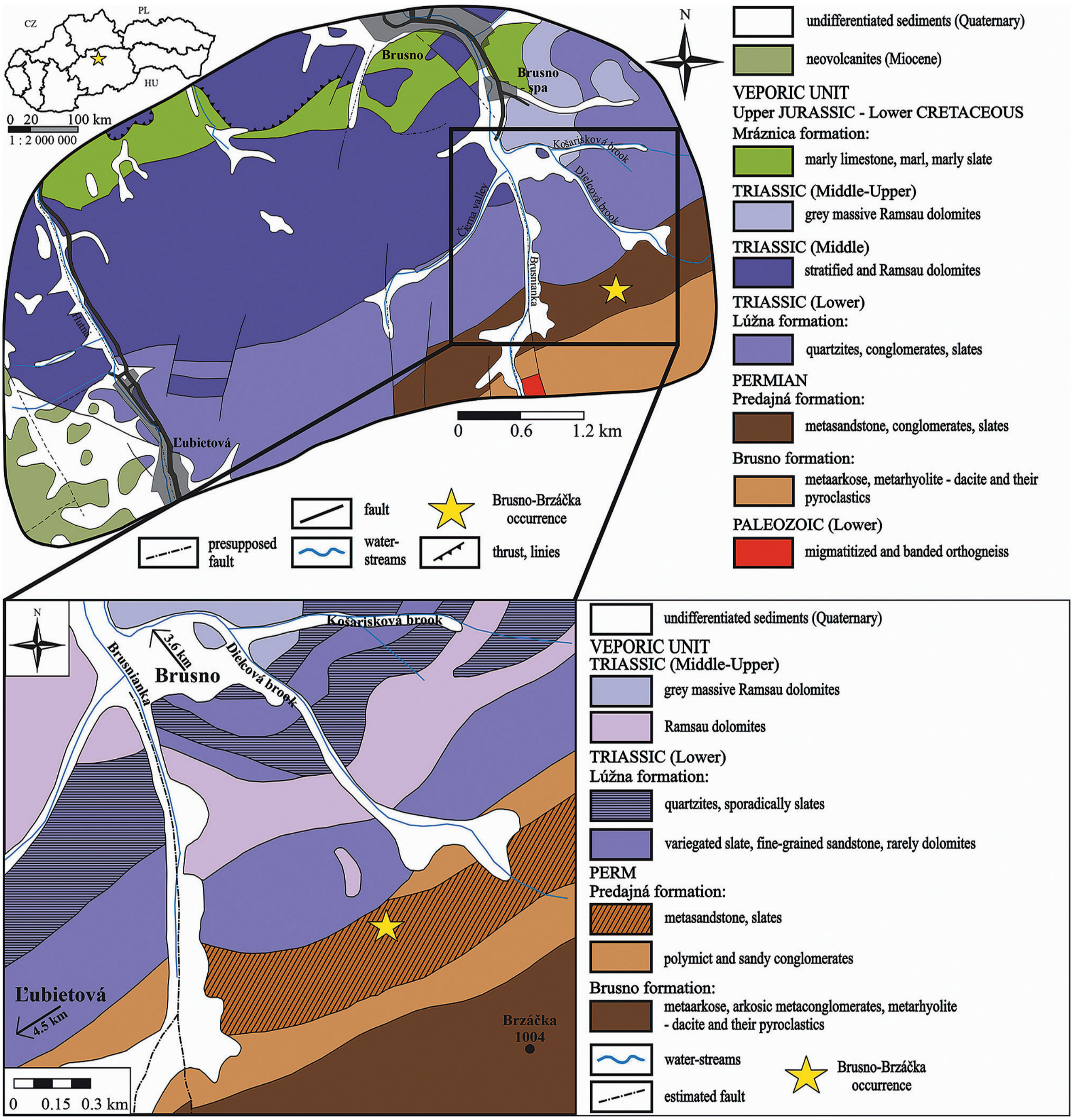

Fig. 1: Geological building of the wider area of the Brusno-Brzáčka occurrence, with its location marking (according to Polák et al., 2003a).

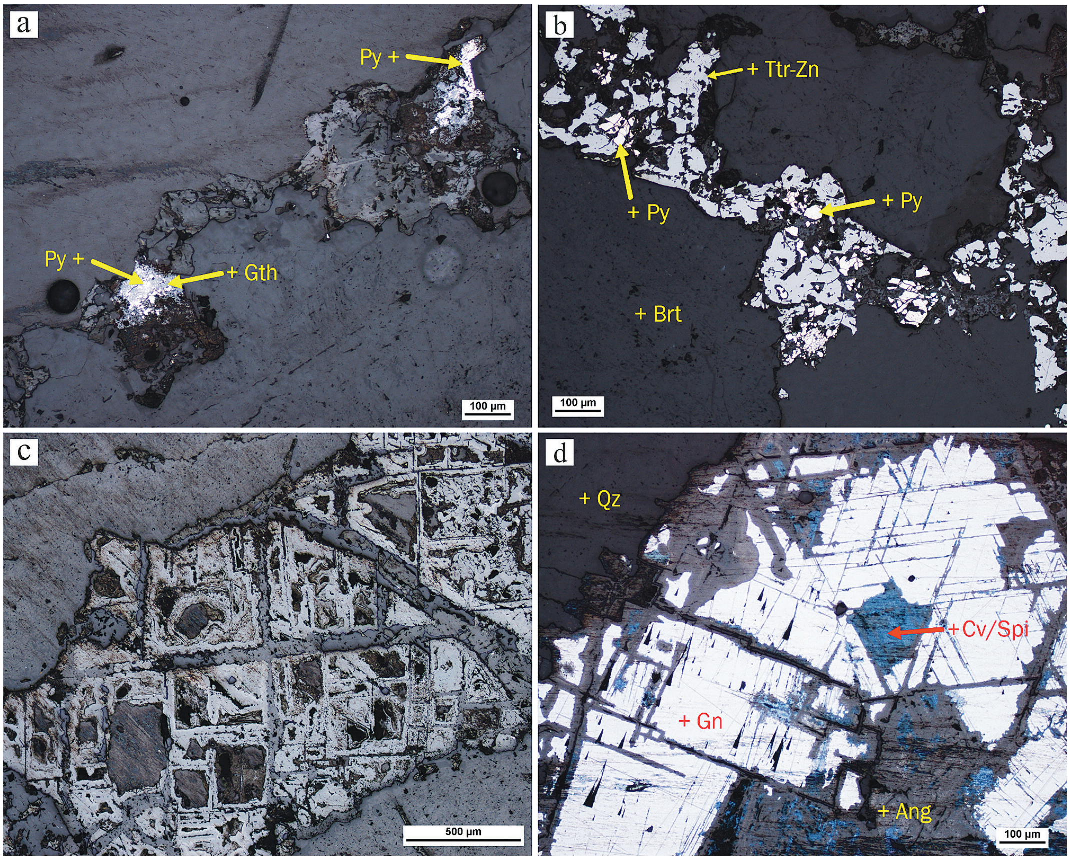

Fig. 2: a) Irregular pyrite (Py) nests partially replaced by goethite (Gth) in a veinlet of unspecified supergene minerals in quartz. b) Tetrahedrite-(Zn) (Ttr-Zn) forms a veinlet in baryte (Brt) and encloses allotriomorphic, cataclased pyrite grains (Py). c) Complete pseudomorphosis of anglesite (lighter, cubic shapes) after galena aggregate in quartz (darker). d) Galena (Gn) is pervasively and along cleavage planes replaced by anglesite (Ang). Covellite and spionkopite aggregates (Cv/Spi, blue) are present in anglesite. All pictures – reflected light, PPL. Photo: Š. Ferenc

Tab. 1 Electron microprobe analyses of galena from the Brusno-Brzáčka occurrence.

an.	1	2	3	4	5	6	7	8	9	10
Pb	84.35	84.45	84.19	82.98	82.88	84.00	85.93	84.67	84.78	85.29
Ag	0.60	0.60	0.63	0.61	0.64	0.52	0.59	0.50	0.61	0.63
Cd	0.02	0.01	0.07	0.00	0.00	0.00	0.00	0.00	0.00	0.00
Cu	0.05	0.04	0.04	0.05	0.01	0.02	0.06	0.06	0.47	0.14
Bi	1.37	1.39	1.19	1.39	1.42	1.40	1.18	1.26	1.32	1.28
As	0.00	0.00	0.00	0.02	0.01	0.00	0.05	0.14	0.00	0.00
Te	0.05	0.05	0.03	0.00	0.00	0.00	0.00	0.00	0.00	0.00
Se	0.22	0.25	0.23	0.26	0.19	0.29	0.05	0.00	0.30	0.02
S	13.65	13.56	13.53	13.65	13.30	13.30	13.58	13.39	13.21	13.30
Cl	0.03	0.05	0.04	0.00	0.00	0.00	0.00	0.00	0.00	0.00
Σ wt. %	100.34	100.40	99.95	98.96	98.46	99.53	101.44	100.02	100.68	100.66
atomic proportions (on the basis of 2 atoms)										
Pb^{2+}	0.960	0.963	0.964	0.950	0.963	0.970	0.974	0.973	0.969	0.979
Ag^{+}	0.013	0.013	0.014	0.013	0.014	0.012	0.013	0.011	0.013	0.014
Cd^{2+}	0.000	0.000	0.001	0.000	0.000	0.000	0.000	0.000	0.000	0.000
Cu^{2+}	0.002	0.001	0.001	0.002	0.000	0.001	0.002	0.002	0.017	0.005
Bi^{3+}	0.015	0.016	0.014	0.016	0.016	0.016	0.013	0.014	0.015	0.015
As^{3+}	0.000	0.000	0.000	0.001	0.000	0.000	0.002	0.004	0.000	0.000
Te^{4+}	0.001	0.001	0.001	0.000	0.000	0.000	0.000	0.000	0.000	0.000
Σ	0.992	0.996	0.995	0.983	0.996	0.999	1.005	1.006	1.016	1.013
Se^{2-}	0.004	0.005	0.004	0.008	0.006	0.009	0.002	0.000	0.009	0.001
S^{2-}	1.004	1.000	1.001	1.010	0.999	0.993	0.995	0.995	0.976	0.987
Cl^{-}	0.002	0.003	0.003	0.000	0.000	0.000	0.000	0.000	0.000	0.000
Σ	1.010	1.008	1.008	1.018	1.006	1.002	0.997	0.995	0.985	0.988

Tetrahedrite-(Zn) is a rare mineral at the studied site. It forms irregular thin veinlets about 2–3 mm long, or individual grains up to 0.15 mm in size in baryte or quartz. It encloses crushed pyrite grains (Fig. 2b). The cracks in the tetrahedrite are filled with anglesite (which indicates an original filling with galena). In the BSE image, an indistinct zonality was detected, where lighter domains (more Zn and Sb) seem to be enclosed in a darker phase (Fig. 3). Chemical composition of tetrahedrite is given in Table 2. In the crystallochemical formula of the studied tetrahedrite, A position (sensu Biagioni et al., 2020) is almost entirely occupied by Cu (≈ 5.98 *apfu*), the silver content of the tetrahedrite is very low (up to 0.07 *apfu* Ag). In the C position, the dominant element is Zn (0.94–1.27 *apfu*), while the Fe and Hg contents were found in the range 0.28–0.54 *apfu* and 0.19–0.50 *apfu*. From the relationships of the main elements occupying the C position, two substitution trends are evident in the studied tetrahedrite (Fig. 4). Less represented is the negative substitution Fe→Zn, near relatively the same Hg content. The negative substitution Fe+Hg→Zn was detected to a greater extent. Position D is also characterized by a very small range of substitutions. The absolutely dominant element is Sb (average 3.59 *apfu*) and less represented is As (average 0.34 *apfu*). Locally, a slightly increased Bi content was detected (max. 0.07 *apfu*). The average chemical composition of tetrahedrite-(Zn) from Brzáčka (26 WDS analyses) can be expressed by the following crystallochemical formula: $(Cu_{5.98}Ag_{0.02})_{\Sigma 6.00}[Cu_{4.00}(Zn_{1.10}Fe_{0.43}Hg_{0.32}Cu_{0.19}Cd_{0.01})_{\Sigma 2.06}]_{\Sigma 6.06}(Sb_{3.59}As_{0.34}Bi_{0.02})_{\Sigma 3.95}S_{12.00}(S_{0.98}\square_{0.02})_{\Sigma 1.00}$.

Quartz is an abundant vein mineral in the locality. Its two generations were identified microscopically. The basic vein mineral is coarse-grained quartz I (grain size up to 0.5 cm) with manifestations of dynamometamorphosis (cataclasis, undulosity, deformation lamellae, migration of grain edges). Quartz II forms veinlets up to 0.5 mm thick, crossing quartz I and accumulations of ore minerals (Fig. 5a). It is not undulose. Accumulations of

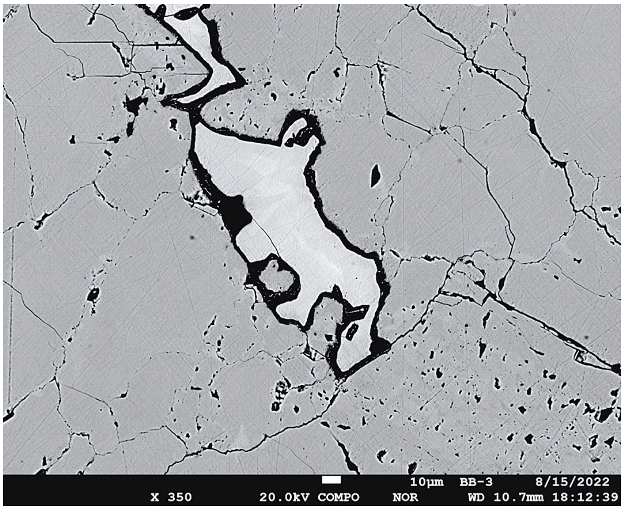

Fig. 3: Irregular veinlet of tetrahedrite-(Zn) (light gray) in baryte (darker). Tetrahedrite is zonal - lighter zones contain more Zn and Sb than darker ones. BSE image. Photo: T. Mikuš.

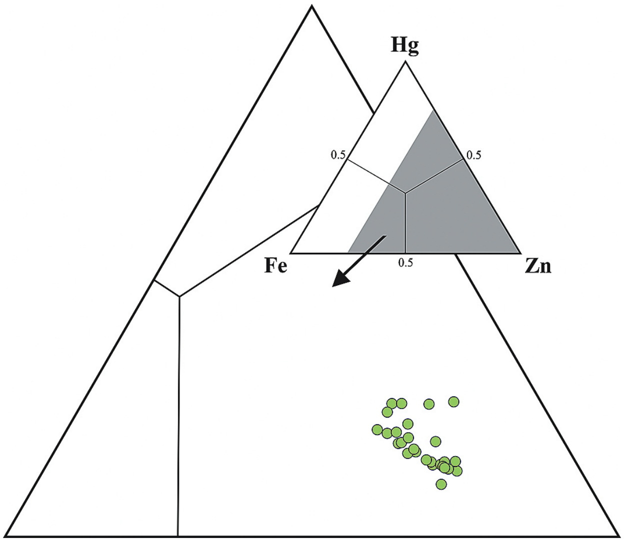

Fig. 4: Composition of the studied tetrahedrite-(Zn) from Brzáčka (*apfu*) in the Fe-Zn-Hg ternary diagram.

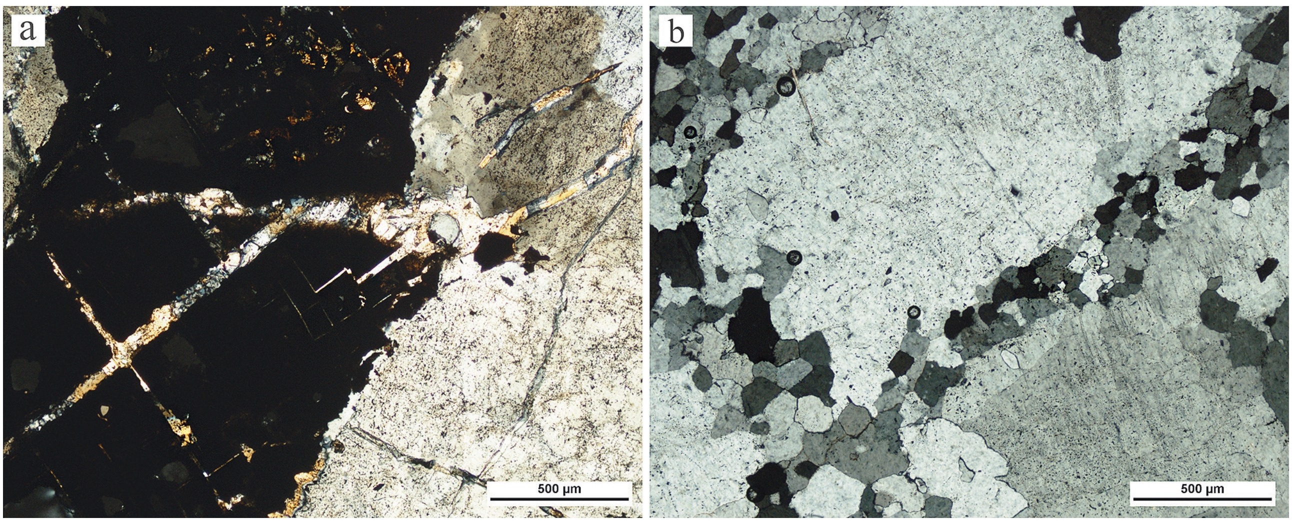

Fig. 5: a) Aggregate of ore minerals (black) in coarsely crystalline quartz I. Ore minerals as well as older quartz are intersected by younger quartz II. b) Hydrothermal baryte with manifestations of dynamometamorphosis (formation of newly formed baryte grains, deformation lamellae). Both images - transmitted light, XPL. Photo: Š. Ferenc.

fine-grained white mica were locally detected in both generations of quartz.

Baryte sometimes forms a substantial (or even the only) part of the gangue. Two of its generations (types, respectively) were observed. Baryte I is coarse-grained (grain size up to 3–4 mm) and shows signs of dynamometamorphism - mainly deformation lamellae (unlike quartz, baryte behaves plastically during deformation, so there are no signs of cataclasis). Dynamic recrystallization is manifested by the formation of newly formed baryte II, which forms veins along the grain boundaries of baryte I, composed of more or less isometric grains reaching around 0.1–0.3 mm in size (Fig. 5b). Chemical composition of the hydrothermal baryte is relatively monotonous (Tab. 3). Slightly elevated concentrations of Sr (0.05–0.09 *apfu*) are stably present. Locally there are other minor ones: Cu up to 0.03 *apfu*, Zn up to 0.01 and Na up to 0.02 *apfu*. Pb concentrations are below the minimum detection limit, but local values of 0.001–0.002 *apfu* were found. However, the increased content of these elements (mainly Cu) can also come from contamination from other mineral phases during analysis (contamination from "baryte footwall" during point WDS analysis). The average chemical composition of hydrothermal baryte from Brzáčka (12 WDS analyses) expresses the following empirical formula: $(Ba_{0.93}Sr_{0.06}Cu_{0.01}Na_{0.01})_{\Sigma 1.01}(SO_4)_{0.99}$.

4.2. Characteristics of the supergene minerals

The oxidation zone of the Brusno-Brzáčka occurrence is poorly developed (appropriate to the weak development of primary mineralization), although the detected spectrum of minerals is relatively diverse. Secondary minerals appear in the form of

Tab. 2 Representative WDS analyses of tetrahedrite-(Zn) from the Brusno-Brzáčka occurrence.

an.	1	2	3	4	5	6	7	8	9	10
Ag	0.10	0.10	0.11	0.10	0.12	0.13	0.10	0.11	0.11	0.13
Cu	38.71	38.31	38.64	39.06	38.26	38.17	38.29	37.86	37.77	39.40
Fe	1.81	1.50	1.71	1.57	1.63	1.47	1.36	1.16	0.92	1.32
Zn	3.67	4.69	4.08	5.02	3.71	3.86	4.68	4.15	4.60	4.41
Cd	0.08	0.07	0.08	0.07	0.09	0.01	0.06	0.08	0.12	0.05
Hg	4.40	3.11	4.01	2.32	5.21	5.76	4.15	5.59	5.97	2.86
Pb	0.00	0.10	0.00	0.04	0.00	0.00	0.00	0.00	0.07	0.05
As	1.49	1.72	1.61	1.66	1.32	1.37	1.70	1.44	1.73	1.43
Sb	26.11	26.06	26.14	26.21	26.30	25.81	25.84	25.89	25.44	26.35
Bi	0.26	0.00	0.00	0.00	0.00	0.13	0.28	0.35	0.00	0.24
S	25.11	24.92	24.92	25.21	25.03	24.80	24.91	24.83	24.53	24.60
Se	0.00	0.00	0.00	0.00	0.01	0.00	0.00	0.00	0.00	0.00
Σ wt. %	101.63	100.47	101.20	101.15	101.55	101.38	101.28	101.36	101.14	100.70
atomic proportions (on the basis of 16 Me atoms)										
Ag^+	0.015	0.016	0.017	0.015	0.018	0.021	0.016	0.017	0.016	0.020
Cu^+	5.985	5.984	5.983	5.985	5.982	5.979	5.984	5.983	5.984	5.980
Σ A	6.000	6.000	6.000	6.000	6.000	6.000	6.000	6.000	6.000	6.000
$Cu^+_{B\ pos.}$	4.000	4.000	4.000	4.000	4.000	4.000	4.000	4.000	4.000	4.000
Fe^{2+}	0.542	0.449	0.511	0.464	0.493	0.444	0.407	0.353	0.277	0.391
Cu^{2+}	0.187	0.091	0.145	0.137	0.145	0.150	0.075	0.106	0.062	0.293
Zn^{2+}	0.938	1.200	1.042	1.266	0.957	0.998	1.197	1.077	1.190	1.120
Cd^{2+}	0.011	0.010	0.012	0.010	0.013	0.002	0.009	0.013	0.018	0.007
Hg^{2+}	0.367	0.259	0.334	0.191	0.438	0.485	0.346	0.473	0.504	0.237
Pb^{2+}	0.000	0.008	0.000	0.003	0.000	0.000	0.000	0.000	0.005	0.004
Σ C	2.045	2.017	2.043	2.070	2.045	2.079	2.034	2.022	2.056	2.051
As^{3+}	0.333	0.385	0.359	0.365	0.298	0.308	0.379	0.325	0.390	0.317
Sb^{3+}	3.586	3.583	3.581	3.549	3.639	3.582	3.549	3.608	3.537	3.593
Bi^{3+}	0.021	0.000	0.000	0.000	0.000	0.011	0.023	0.028	0.000	0.019
Σ D	3.940	3.967	3.940	3.915	3.937	3.900	3.950	3.961	3.927	3.929
S^{2-}	12.000	12.000	12.000	12.000	11.997	12.000	12.000	12.000	12.000	12.000
Se^{2-}	0.000	0.000	0.000	0.000	0.003	0.000	0.000	0.000	0.000	0.000
Σ Y	12.000	12.000	12.000	12.000	12.000	12.000	12.000	12.000	12.000	12.000
S^{2-}	1.099	1.012	0.968	0.970	1.154	1.070	0.994	1.137	0.951	0.739
□			0.032	0.030			0.006		0.049	0.261
Σ Z	1.099	1.012	1.000	1.000	1.154	1.070	1.000	1.137	1.000	1.000

veins, clusters and irregular grains mainly in quartz. Locally, they form complete pseudomorphs after aggregates of primary ore minerals. Supergene weathering products are represented by baryte, anglesite, bismutite, pyromorphite, mimetite, covellite and spionkopite.

Baryte of supergene origin is relatively rare at the site. It forms irregular veinlets crossing anglesite and quartz (Fig. 6a). The chemical composition of baryte was studied only informatively (1 WDS analysis; Tab. 3). Contrary to the hydrothermal baryte, supergene one is characterized by a low content of other elements: Pb 0.003 *apfu* and Sr up to 0.002 *apfu*. The empirical formula of baryte approaches the ideal $BaSO_4$.

Anglesite is a relatively abundant supergene mineral in the studied occurrence. It partially or completely replaces galena, the shape of its irregular aggregates copies the shape of the original galena aggregates (Fig. 6b,c). It is most often associated with its variety Ba-rich anglesite. The studied anglesite (Tab. 4) contains minor other elements, Bi (up to 0.12 *apfu*), Cu (up to 0.08 *apfu*) and Ba (up to 0.07 *apfu*). In addition to dominant sulfur, Se enters the anion position in a minor amount (up to 0.03 *apfu*). The empirical anglesite formula from Brzáčka (5 WDS microanalyses) can be expressed as follows: $(Pb_{0.92}Ba_{0.05}Bi_{0.04}Cu_{0.02}Fe_{0.01})_{\Sigma 1.03}(SO_4)_{0.99}$.

The mineralogically noteworthy phase of the studied site is the Ba-rich anglesite. It is often intergrown with slightly younger anglesite (without Ba), forming irregular aggregates (Fig. 6c). In the chemical composition of the transitional mineral phase of the baryte-anglesite series (Tab. 5), we detected minor contents of Zn (max. 0.01 *apfu*), Fe (up to 0.02 *apfu*), Sr (up to 0.02 *apfu*), Cu (up to 0.03 *apfu*) and locally increased Bi (up to 0.13 *apfu*). Ba-rich anglesite is characterized by significant Ba → Pb substitution (0.12–0.51 *apfu* Ba; 0.50–0.88 *apfu* Pb). Selenium (up to 0.06 *apfu*) occasionally enters the anionic X position. The average chemical composition of the studied Ba-rich anglesite (16 point WDS analyses) expresses an empirical formula $(Pb_{0.66}Ba_{0.34})_{\Sigma 1.00}(SO_4)$. Based on the nomenclature rule of 50 %, the studied mineral phase lies practically only in the anglesite field (Fig. 7).

Accessory mineral of the Brzáčka locality is **bismutite**, $Bi_2(CO_3)O_2$, which forms veinlets in anglesite (Fig. 6a, 8). Microprobe analyses of bismutite revealed significant enrichment in Pb (up to 0.24 *apfu*) and Sb (up to 0.08 *apfu*), in a lesser extent Fe (up to 0.04 *apfu*) and Cu (up to 0.01 *apfu*), at the expense of Bi_2O_3 content (max. 1.58 *apfu* Bi). A slightly increased content of S was detected in the anionic position (up to 0.05 *apfu*; Tab. 6). The average empirical formula of studied mineral phase (2 WDS analyses) is: $(Bi_{1.57}Pb_{0.23}Sb_{0.08}Fe_{0.04}Cu_{0.01})_{\Sigma 1.93}[(CO_3)_{0.90}(SO_4)_{0.05}(SeO_4)_{0.01}(PO_4)_{0.01}]_{\Sigma 0.97}O_2$.

Pyromorphite is locally found in association with younger anglesite (Fig. 9a). The studied pyromorphite differs from the ideal chemical composition, $Pb_5(PO_4)_3Cl$, by the presence of increased Fe contents (0.09–0.15 *apfu*) and minor contents of Sr, Sb and Bi (up to 0.06 *apfu*; for each element separately). Interesting are the significant Cu contents varying in the range of 0.14 to 0.28 *apfu*. In addition to the majority of P (1.88–2.82 *apfu*), S (0.02–0.22 *apfu*) and As (up to 0.68 *apfu*) are also present at the anion position. The significant As → P substitution was also detected (0.52–1.22 *apfu* As; Fig. 10). Chlorine dominates in all analyzes of pyromorphite, its amount ranges from 0.80 to 0.92 *apfu*. The chemical composition of pyromorphite is shown in Table 7. The average empirical formula of pyromorphite (7 WDS microanalyses) from

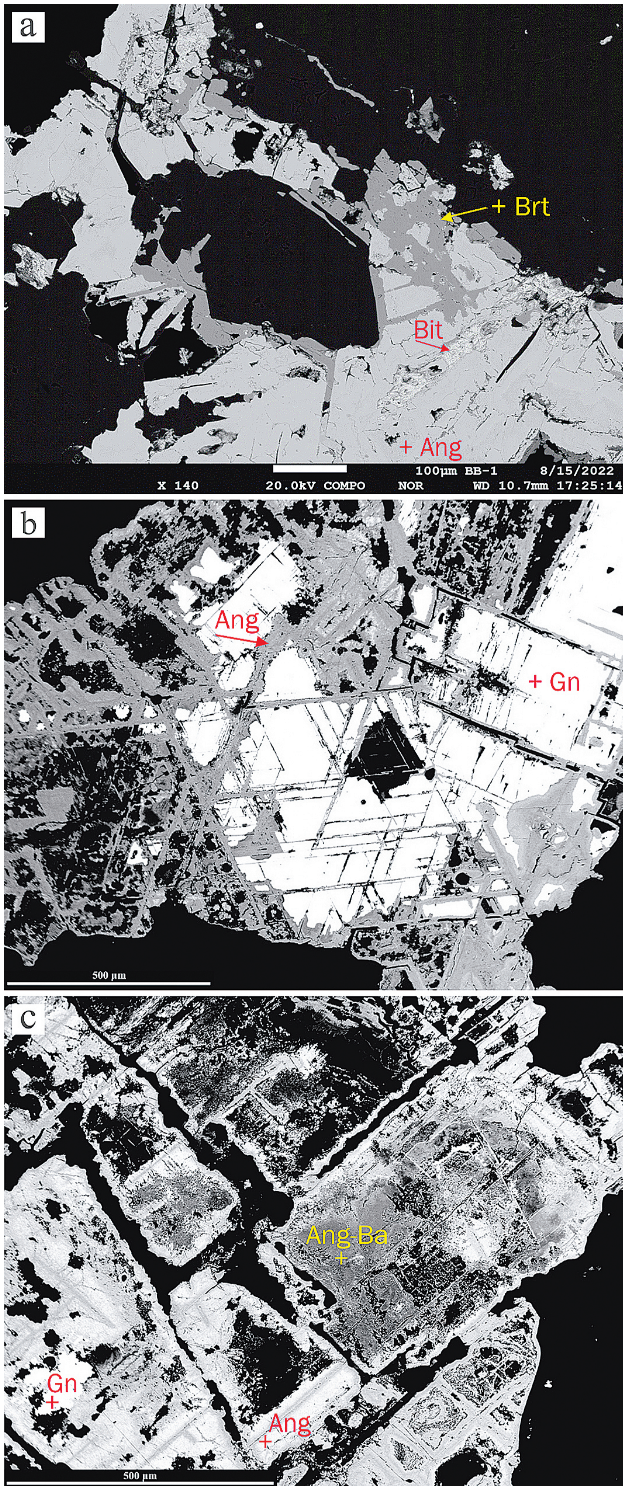

Fig 6: a) Bismutite veinlet (Bit) in anglesite (Ang). Baryte (Brt) rims and cut the anglesite aggregate. b) Galena (Gn) replaced by anglesite (Ang) along cleavage. c) Anglesite (Ang) and Ba-rich anglesite (Ang-Ba) pseudomorphs after cubic galena. BSE pictures. Photo: T. Mikuš.

Tab. 3 Electron microprobe analyses of baryte. Brt – hydrothermal phase, Brt* – supergene phase.

an.	1	2	3	4	5	6	7	8	9	10
mineral	Brt*	Brt	Brt	Brt	Brt	Brt	Brt	Brt	Brt	Brt
SO_3	33.53	33.24	33.61	34.66	33.78	34.93	35.11	35.41	34.66	34.81
Sb_2O_5	0.03	0.02	0.00	n. a.	n. a.	n. a.	n. a.	n. a.	n. a.	n. a.
Al_2O_3	0.03	0.13	0.02	0.03	0.10	0.07	0.05	0.08	0.09	0.12
Fe_2O_3	0.02	0.11	0.04	0.02	0.03	0.02	0.00	0.03	0.01	0.00
Bi_2O_3	0.00	0.00	1.73	n. a.	n. a.	n. a.	n. a.	n. a.	n. a.	n. a.
SrO	0.08	2.21	2.12	2.73	2.57	2.50	2.39	3.93	3.93	2.54
BaO	64.20	60.20	61.74	62.95	60.96	62.69	62.50	61.16	61.23	62.51
ZnO	0.08	0.02	0.00	0.24	0.12	0.14	0.14	0.00	0.03	0.00
CuO	0.02	0.00	0.00	1.10	0.85	0.61	1.16	0.00	0.00	0.07
PbO	0.28	0.15	0.12	0.00	0.00	0.00	0.01	0.00	0.00	0.00
Na_2O	n. a.	n. a.	n. a.	0.12	0.19	0.25	0.27	0.06	0.06	0.17
Σ wt. %	98.26	96.08	99.37	101.85	98.60	101.21	101.63	100.67	100.01	100.22
atomic proportions										
Sb^{5+}	0.001	0.001	0.000	n. a.	n. a.	n. a.	n. a.	n. a.	n. a.	n. a.
Al^{3+}	0.001	0.006	0.001	0.001	0.005	0.003	0.002	0.004	0.004	0.005
Fe^{3+}	0.002	0.007	0.003	0.001	0.002	0.001	0.000	0.002	0.001	0.000
Bi^{3+}	0.000	0.000	0.036	n. a.	n. a.	n. a.	n. a.	n. a.	n. a.	n. a.
Sr^{2+}	0.002	0.051	0.048	0.060	0.058	0.055	0.052	0.086	0.087	0.056
Ba^{2+}	0.996	0.941	0.942	0.935	0.931	0.930	0.922	0.902	0.918	0.935
Zn^{2+}	0.002	0.001	0.000	0.007	0.003	0.004	0.004	0.000	0.001	0.000
Cu^{2+}	0.001	0.000	0.000	0.031	0.025	0.017	0.033	0.000	0.000	0.002
Pb^{2+}	0.003	0.002	0.001	0.000	0.000	0.000	0.000	0.000	0.000	0.000
Na^{+}	n. a.	n. a.	n. a.	0.009	0.014	0.018	0.020	0.004	0.004	0.013
Σ A	1.008	1.008	1.031	1.045	1.039	1.029	1.033	0.998	1.015	1.011
S^{6+}	0.996	0.994	0.981	0.985	0.987	0.991	0.991	0.999	0.994	0.996

Atomic proportions were calculated on the basis of 4 oxygen atoms; n. a. – not analysed.

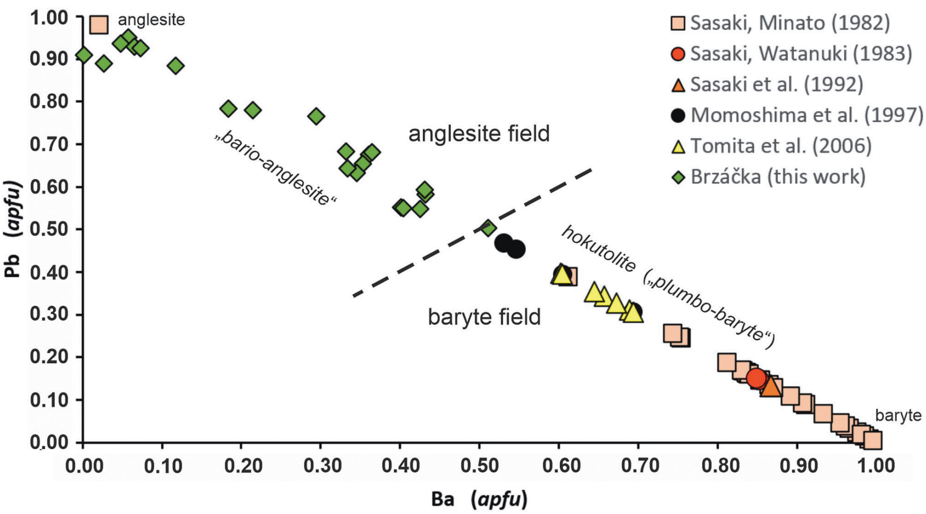

Fig. 7: Ba vs. Pb contents in Ba-rich anglesite from Brzáčka compared to Pb-rich baryte (*"hokutolite"*).

Brzáčka is: $(Pb_{4.47}Ca_{0.19}Cu_{0.16}Fe_{0.10}Sb_{0.02}Bi_{0.02}Sr_{0.02}Zn_{0.02}Ba_{0.01})_{\Sigma 5.00}[(PO_4)_{2.24}(AsO_4)_{0.42}(CO_2)_{0.25}(SO_4)_{0.09}]_{\Sigma 3.00}(Cl_{0.90}OH_{0.10})_{\Sigma 1.00}$.

Mimetite was most often found in association with baryte and anglesite (Fig. 9b). Representative analyses of mimetite are given in a Table 8. In addition to dominant Pb, Bi (0.02–0.05 *apfu*), Sr (up to 0.07 *apfu*) and Sb (0.01–0.04 *apfu*) enter the cationic position. Low contents of Cu (up to 0.01 *apfu*), Ba (up to 0.04 *apfu*) and Fe (up to 0.04 *apfu*) were found locally. The anionic position is dominantly occupied by As (2.56–2.64 *apfu*), the content of S is significantly increased (0.18–0.20 *apfu*). In contrast to pyromorphite, isomorphic substitution P → As is practically absent in mimetite (0.04–0.07 *apfu* P; Fig. 10). The Cl content ranges from 0.95 to 0.99 *apfu*. The average crystal chemical formula of mimetite (10 WDS analyses) can be expressed as $(Pb_{4.89}Bi_{0.03}$

$Sr_{0.03}Fe_{0.02}Sb_{0.01}Cu_{0.01}Ba_{0.01})_{\Sigma 5.00}[(AsO_4)_{2.61}(SO_4)_{0.19}(PO_4)_{0.05}(CO_2)_{0.15}]_{\Sigma 3.00}(Cl_{0.97}OH_{0.03})_{\Sigma 1.00}$.

Goethite is a relatively common mineral phase in small amounts. It most often forms dark brown and rusty thin coatings on the surface of mineralized samples. Unspecified Fe oxides form yellowish-brown earthy masses in cavities of quartz (pseudomorphoses after original pyrite aggregates).

4.3. Mineral phases of the Cu-S system

Minerals of the Cu-S system form fine coatings and fissure fillings of various shades of blue. They replace galena along the cracks and edges of its aggregates (Fig. 2d) in association with anglesite or Ba-rich anglesite. A relatively abundant mineral at the Brzáčka locality is **covellite**, with a ratio of cations/anions ~ 0.99/1 (1/1 in ideal covellite). In its chemical composition (Tab. 9), enrichment of Ag (up to 0.05 *apfu*) and a small content of other elements (Zn, Se – less than 0.01 *apfu* in total) was detected. The average empirical formula of covellite (13 WDS analyses) can be expressed as $(Cu_{3.94}Ag_{0.06})_{\Sigma 4}Cu_{2.06}(S_{1.99}Se_{0.01})_{\Sigma 2}S_{4.07}$. The cation/anion ratio in the mineral phase close to **spionkopite** ranges from 1.28–1.30/1 (1.4/1 in ideal spionkopite). The studied

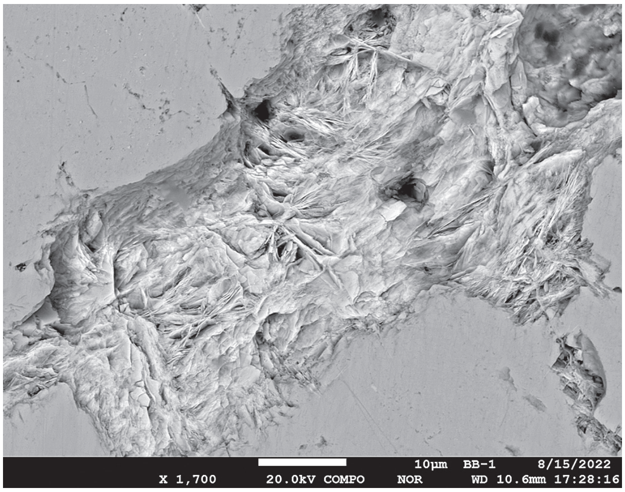

Fig. 8: Detailed view of a bismutite aggregate hosted by anglesite (dark gray, compact), BSE image. Photo: T. Mikuš.

Tab. 4 Electron microprobe analyses of anglesite from the Brusno-Brzáčka occurrence.

an.	1	2	3	4	5	6
SO_3	26.43	25.94	25.67	25.78	25.96	26.05
SeO_3	n. a.	0.92	0.60	0.00	0.00	0.00
P_2O_5	n. a.	0.00	0.00	0.02	0.05	0.02
Sb_2O_5	n. a.	0.00	0.02	0.01	0.00	0.01
Fe_2O_3	0.08	0.06	0.00	0.22	0.13	0.00
Bi_2O_3	n. a.	1.80	4.66	0.39	0.21	0.22
CuO	0.44	2.13	0.28	0.04	0.02	0.00
ZnO	0.07	0.00	0.08	0.12	0.06	0.05
SrO	0.00	0.08	0.00	0.37	0.20	0.36
BaO	2.96	0.11	1.38	3.29	3.67	2.39
PbO	70.89	68.66	67.15	68.12	67.84	68.16
Σ wt. %	100.87	99.70	99.83	98.36	98.13	97.25
			atomic proportions			
Sb^{5+}	n. a.	0.000	0.001	0.000	0.000	0.000
Fe^{3+}	0.007	0.005	0.000	0.018	0.011	0.000
Bi^{3+}	n. a.	0.047	0.123	0.011	0.006	0.006
Cu^{2+}	0.017	0.079	0.010	0.002	0.001	0.000
Zn^{2+}	0.003	0.000	0.003	0.004	0.002	0.002
Sr^{2+}	0.000	0.002	0.000	0.011	0.006	0.011
Ba^{2+}	0.058	0.002	0.027	0.065	0.073	0.048
Pb^{2+}	0.950	0.909	0.890	0.930	0.926	0.936
Σ A	1.033	1.044	1.054	1.041	1.024	1.003
S^{6+}	0.986	0.956	0.948	0.980	0.986	0.996
Se^{6+}	n. a.	0.029	0.019	0.000	0.000	0.000
P^{5+}	n. a.	0.000	0.000	0.001	0.002	0.001
Σ X	0.986	0.985	0.967	0.980	0.989	0.997

Calculation of atomic proportions is based on 4 oxygen atoms; n. a. – not analysed.

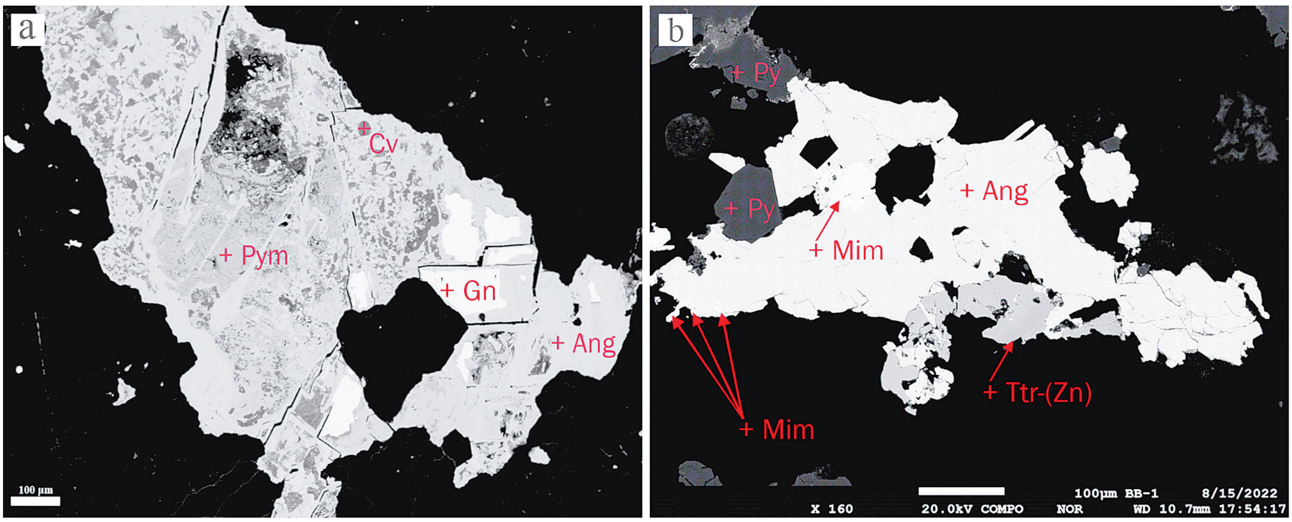

Fig. 9: a) Pyromorphite aggregate (Pym) rimmed and cut by anglesite (Ang). Covellite (Cv) forms fine-grained aggregates and galena (Gn) forms relicts in anglesite. b) Mimetite (Mim) forms irregular grains in anglesite (Ang), which is in asossociation with pyrite (Py). The replacing of tetrahedrite-(Zn) (Ttr-Zn) by anglesite, indicates original replacing of tetrahedrite by galena. BSE images. Photo: T. Mikuš.

Tab. 5 Electron microprobe analyses of Ba-rich anglesite from the Brusno-Brzáčka occurrence.

an.	1	2	3	4	5	6	7	8	9	10
SO_3	29.16	29.92	28.74	27.18	27.10	25.84	25.95	25.88	25.56	26.02
SeO_3	n. a.	n. a.	n. a.	n. a.	n. a.	n. a.	1.1	1.29	1.69	1.99
Fe_2O_3	0.03	0.01	0.02	0.10	0.05	0.00	0.11	0.07	0.00	0.15
Bi_2O_3	n. a.	n. a.	n. a.	n. a.	n. a.	n. a.	3.90	4.87	5.27	0.30
CuO	0.02	0.09	0.00	0.11	0.11	0.07	0.11	0.13	0.22	0.13
ZnO	0.00	0.10	0.00	0.01	0.00	0.00	0.07	0.17	0.13	0.12
SrO	0.00	0.00	0.00	0.00	0.00	0.00	0.00	0.02	0.00	0.00
BaO	24.31	29.51	18.43	19.15	19.29	14.88	22.73	21.60	21.81	18.65
PbO	47.60	42.29	55.08	52.17	52.55	56.41	42.65	43.25	43.15	50.31
Σ wt. %	101.12	101.92	102.27	98.72	99.10	97.20	96.60	97.29	97.83	97.68
					atomic proportions					
Fe^{3+}	0.002	0.001	0.002	0.008	0.004	0.000	0.009	0.005	0.000	0.012
Bi^{3+}	n. a.	n. a.	n. a.	n. a.	n. a.	n. a.	0.100	0.123	0.133	0.008
Cu^{2+}	0.001	0.003	0.000	0.004	0.004	0.003	0.004	0.005	0.008	0.005
Zn^{2+}	0.000	0.003	0.000	0.000	0.000	0.000	0.002	0.006	0.005	0.004
Sr^{2+}	0.000	0.000	0.000	0.000	0.000	0.000	0.000	0.001	0.000	0.000
Ba^{2+}	0.433	0.511	0.333	0.361	0.364	0.294	0.426	0.401	0.405	0.353
Pb^{2+}	0.582	0.503	0.683	0.676	0.682	0.766	0.549	0.552	0.550	0.654
Σ A	1.017	1.022	1.017	1.049	1.054	1.063	1.089	1.093	1.100	1.036
S^{6+}	0.993	0.992	0.992	0.981	0.979	0.978	0.930	0.920	0.907	0.942
Se^{6+}	n. a.	n. a.	n. a.	n. a.	n. a.	n. a.	0.029	0.034	0.051	0.061
Σ X	0.993	0.992	0.992	0.981	0.979	0.978	0.959	0.954	0.958	1.003

Atomic proportions were calculated on the basis of 4 oxygen atoms; n. a. – not analysed.

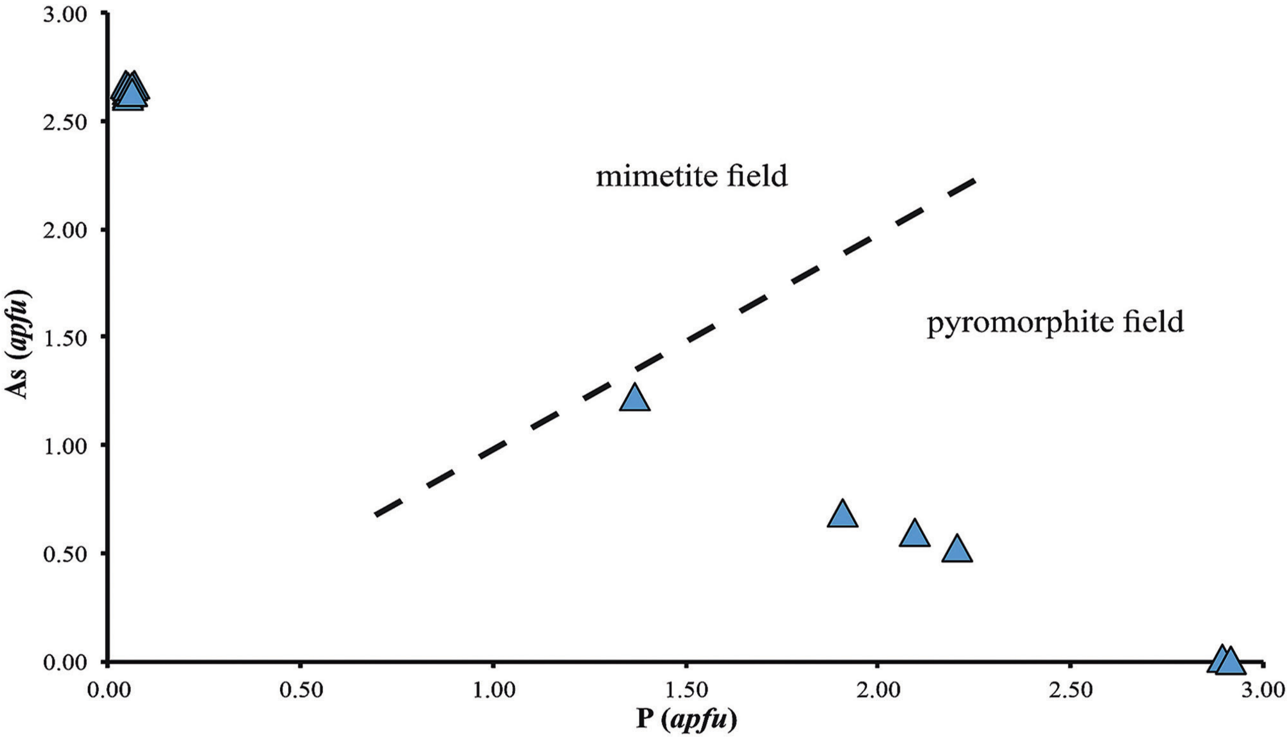

Fig. 10: Variations of the anionic position of pyromorphite and mimetite in the diagram P vs. As.

mineral phase differs from the ideal chemical composition by the presence of additional components Ag (up to 0.47 *apfu*), Bi (up to 0.04) and Zn (max. 0.01 *apfu*). From the average of two point WDS analyses (Tab. 9), the chemical composition of spionkopite from Brzáčka can be expressed as $(Cu_{14.56}Ag_{0.44})_{\Sigma 15.00}(Cu_{4.44}Bi_{0.04}Zn_{0.01})_{4.49}(S_{1.93}Se_{0.07})_{\Sigma 2.00}(S)_{13.15}$. The both minerals formulae are expressed in an extended form (sensu Goble, 1985).

Tab. 6 WDS analyses of bismutite from the Brusno-Brzáčka occurrence.

an.	1	2
SO_3	0.78	0.80
SeO_3	0.16	0.14
P_2O_5	0.17	0.18
As_2O_5	0.20	0.01
Sb_2O_5	2.38	2.25
CO_{2*}	9.43	9.41
SiO_2	0.05	0.01
Al_2O_3	0.01	0.02
Fe_2O_3	0.47	0.60
Bi_2O_3	74.43	76.10
BaO	0.00	0.17
ZnO	0.10	0.01
CuO	0.13	0.18
PbO	11.14	10.88
Σ wt. %	99.45	100.77
atomic proportions		
Sb^{5+}	0.082	0.076
Fe^{3+}	0.031	0.039
Bi^{3+}	1.568	1.579
Ba^{2+}	0.000	0.005
Zn^{2+}	0.006	0.000
Cu^{2+}	0.008	0.011
Pb^{2+}	0.237	0.228
Σ	1.932	1.938
S^{6+}	0.046	0.047
Se^{6+}	0.008	0.007
P^{5+}	0.006	0.006
As^{5+}	0.004	0.000
C^{4+}	0.900	0.900
Si^{4+}	0.004	0.001
Σ	0.968	0.961
O	2.000	2.000

Atomic proportions were normalized based on 2 cations; content of CO_2 was calculated on the basis of stoichiometry and charge balance.

Tab. 7 Electron microprobe analyses of pyromorphite from Brzáčka occurrence.

an.	1	2	3	4	5	6	7	mean
SO_3	0.00	0.01	0.11	0.91	1.36	0.65	0.87	0.00
P_2O_5	15.81	15.91	15.47	10.97	10.21	11.70	6.86	13.35
As_2O_5	0.04	0.07	0.05	5.03	5.96	4.47	9.95	2.60
CO_{2calc}	0.69	0.74	0.54	0.81	0.76	1.04	1.39	0.00
SiO_2	0.00	0.00	0.00	0.00	0.00	0.00	0.00	0.00
Sb_2O_3	0.00	0.05	0.00	0.29	0.45	0.25	0.41	0.17
Bi_2O_3	0.05	0.15	0.11	0.47	0.76	0.40	0.71	0.32
CaO	2.05	2.04	1.69	0.00	0.00	0.10	0.00	0.98
SrO	0.00	0.00	0.00	0.08	0.46	0.25	0.44	0.13
BaO	0.01	0.00	0.02	0.00	0.26	0.14	0.19	0.07
ZnO	0.02	0.14	0.00	0.13	0.14	0.20	0.11	0.10
CuO	0.04	0.02	0.00	1.63	1.61	1.73	1.72	0.84
PbO	79.59	79.42	78.95	77.43	75.71	77.73	73.67	78.14
FeO_{total}	0.28	0.55	0.15	0.44	0.69	0.82	0.86	0.49
H_2O_{calc}	0.00	0.00	0.00	0.00	0.00	0.00	0.09	0.00
Cl	2.61	2.76	2.41	2.42	2.38	2.39	2.32	2.49
O=F	0.00	0.00	0.00	0.00	0.00	0.00	0.00	0.00
O=Cl	-0.59	-0.62	-0.54	-0.55	-0.54	-0.54	-0.52	–0.56
Σ wt. %	100.60	101.23	98.95	100.06	100.21	101.32	99.05	99.64
atomic proportions								
S^{6+}	0.000	0.002	0.018	0.149	0.222	0.103	0.144	0.09
P^{5+}	2.798	2.783	2.819	2.034	1.877	2.100	1.285	2.24
As^{5+}	0.004	0.008	0.006	0.575	0.676	0.496	1.151	0.42
C^{4+}	0.197	0.208	0.157	0.242	0.225	0.302	0.421	0.25
Si^{4+}	0.000	0.000	0.000	0.000	0.000	0.000	0.000	0.00
Σ T	3.000	3.000	3.000	3.000	3.000	3.000	3.000	3.00
Sb^{3+}	0.000	0.004	0.000	0.026	0.040	0.022	0.037	0.02
Bi^{3+}	0.003	0.008	0.006	0.027	0.042	0.022	0.040	0.02
Ca^{2+}	0.459	0.452	0.390	0.000	0.000	0.023	0.000	0.19
Sr^{2+}	0.000	0.000	0.000	0.011	0.058	0.030	0.056	0.02
Ba^{2+}	0.001	0.000	0.002	0.000	0.022	0.011	0.016	0.01
Zn^{2+}	0.003	0.021	0.000	0.021	0.022	0.031	0.017	0.02
Cu^{2+}	0.006	0.003	0.000	0.270	0.264	0.277	0.287	0.16
Pb^{2+}	4.479	4.417	4.575	4.564	4.425	4.437	4.387	4.47
Fe^{2+}	0.049	0.095	0.028	0.081	0.126	0.146	0.158	0.10
Σ M	5.000	5.000	5.000	5.000	5.000	5.000	5.000	5.00
OH^-_{calc}	0.075	0.034	0.121	0.103	0.125	0.141	0.130	0.10
F^-	0.000	0.000	0.000	0.000	0.000	0.000	0.000	0.00
Cl^-	0.925	0.966	0.879	0.897	0.875	0.859	0.870	0.90
Σ X	1.000	1.000	1.000	1.000	1.000	1.000	1.000	1.00

Atomic proportions were calculated on the basis of M = 5 cations and $OH^- + F^- + Cl^- = 1$ apfu (Pasero et al. 2010). CO_2 and H_2O contents calculated on the basis of ideal stoichiometry; mean – diameter of 7 point WDS analyzes.

5. DISCUSSION AND CONCLUSIONS

5.1. Evolution and genesis of primary (hydrothermal) mineralization

A consequence of the weak development of mineralization is the mutual isolation of individual aggregates of ore minerals or the mineral phases themselves, which does not allow relevant determination of their mutual microstructural relationships. Another reason is the poor terrain exposure – mineralised samples were taken at points and more or less randomly, without the possibility to study mineralization directly in the outcrops or in the adit. Nevertheless, it is possible to roughly determine its development on the basis of the relationships of primary and supergene minerals, also on the basis of correlation with succession schemes of more significant and better studied ore deposits/occurrences in the Veporic, or in Gemeric Units.

Tab. 8 Electron microprobe analyses of mimetite from the Brusno-Brzáčka occurrence.

an.	1	2	3	4	5	6	7	8	9	10
SO_3	1.08	1.05	1.02	1.01	1.11	1.02	1.07	0.99	1.00	1.04
P_2O_5	0.25	0.24	0.21	0.32	0.25	0.21	0.24	0.26	0.28	0.30
As_2O_5	20.36	20.41	20.33	21.14	20.11	20.53	20.36	20.07	20.35	20.45
CO_{2calc}	0.60	0.46	0.39	0.34	0.48	0.38	0.40	0.53	0.38	0.50
SiO_2	0.00	0.00	0.00	0.00	0.00	0.00	0.00	0.00	0.00	0.00
Sb_2O_3	0.05	0.13	0.07	0.07	0.06	0.07	0.03	0.03	0.11	0.04
Bi_2O_3	0.41	0.60	0.55	0.41	0.77	0.62	0.53	0.51	0.37	0.50
CaO	0.00	0.00	0.00	0.01	0.01	0.01	0.01	0.00	0.00	0.01
SrO	0.21	0.23	0.32	0.00	0.10	0.00	0.34	0.00	0.51	0.53
BaO	0.09	0.00	0.00	0.00	0.00	0.02	0.45	0.08	0.09	0.00
ZnO	0.00	0.11	0.00	0.00	0.00	0.00	0.00	0.06	0.00	0.03
CuO	0.04	0.03	0.07	0.00	0.00	0.02	0.06	0.00	0.00	0.07
PbO	75.75	74.44	73.34	76.51	74.05	74.39	73.33	74.12	73.13	74.77
FeO_{total}	0.12	0.00	0.02	0.21	0.16	0.08	0.00	0.14	0.12	0.00
H_2O_{calc}	0.03	0.02	0.03	0.03	0.00	0.01	0.03	0.01	0.01	0.01
Cl	2.34	2.36	2.26	2.35	2.38	2.35	2.27	2.36	2.34	2.42
O=F	0.00	0.00	0.00	0.00	0.00	0.00	0.00	0.00	0.00	0.00
O=Cl	–0.53	–0.53	–0.51	–0.53	–0.54	–0.53	–0.51	–0.53	–0.53	–0.54
Σ wt. %	100.82	99.52	98.10	101.86	98.96	99.18	98.61	98.61	98.17	100.11
					atomic proportions					
S^{6+}	0.20	0.19	0.19	0.18	0.20	0.19	0.20	0.18	0.19	0.19
P^{5+}	0.05	0.05	0.04	0.07	0.05	0.04	0.05	0.05	0.06	0.06
As^{5+}	2.56	2.61	2.63	2.64	2.58	2.64	2.62	2.59	2.63	2.59
C^{4+}	0.20	0.15	0.13	0.11	0.16	0.13	0.13	0.18	0.13	0.16
Σ T	3.00	3.00	3.00	3.00	3.00	3.00	3.00	3.00	3.00	3.00
Sb^{3+}	0.00	0.01	0.01	0.01	0.01	0.01	0.00	0.00	0.01	0.00
Bi^{3+}	0.03	0.04	0.04	0.03	0.05	0.04	0.03	0.03	0.02	0.03
Ca^{2+}	0.00	0.00	0.00	0.00	0.00	0.00	0.00	0.00	0.00	0.00
Sr^{2+}	0.03	0.03	0.05	0.00	0.01	0.00	0.05	0.00	0.07	0.07
Ba^{2+}	0.01	0.00	0.00	0.00	0.00	0.00	0.04	0.01	0.01	0.00
Zn^{2+}	0.00	0.02	0.00	0.00	0.00	0.00	0.00	0.01	0.00	0.01
Cu^{2+}	0.01	0.00	0.01	0.00	0.00	0.00	0.01	0.00	0.00	0.01
Pb^{2+}	4.90	4.89	4.89	4.92	4.89	4.93	4.86	4.92	4.86	4.87
Fe^{2+}	0.02	0.00	0.00	0.04	0.03	0.02	0.00	0.03	0.03	0.00
Σ M	5.00	5.00	5.00	5.00	5.00	5.00	5.00	5.00	5.00	5.00
OH^-_{calc}	0.05	0.02	0.05	0.05	0.01	0.02	0.05	0.01	0.02	0.01
F^-	0.00	0.00	0.00	0.00	0.00	0.00	0.00	0.00	0.00	0.00
Cl^-	0.95	0.98	0.95	0.95	0.99	0.98	0.95	0.99	0.98	0.99
Σ X	1.00	1.00	1.00	1.00	1.00	1.00	1.00	1.00	1.00	1.00

Atomic proportions were calculated on the basis of M = 5 cations and $OH^- + F^- + Cl^- = 1$ *apfu* (Pasero et al. 2010).
CO_2 and H_2O contents calculated on the basis of ideal stoichiometry; mean – diameter of 10 point WDS analyzes.

Within the **hydrothermal phase** of the development of mineralization, the oldest minerals are coarse-grained **quartz I** (main gangue mineral) and **pyrite** (***mineralization period I***). Afterwards, **baryte** was deposited (***mineralization period II***). In the period III, **tetrahedrite-(Zn)** and **chalcopyrite** were formed. Precipitation of **galena** took place already in the period IV. Clusters of primary ore minerals (also complete pseudomorphs of supergene minerals after them) are cut by thin veinlets of **quartz II** (*period V*).

The character of hydrothermal mineralization at the studied site is similar to that at the nearby Ľubietová-Peklo occurrence in the Northern Veporic (Ferenc et al., 2019), or at the occurrences of siderite-sulfidic mineralization at Uderiná, Lovinobaňa and Cinobaňa in the Southern Veporic Unit (Ferenc et al., 2014). It can also be roughly compared with the development of siderite-sulfidic hydrothermal mineralization in the Spišsko-Gemerské Rudohorie in the Gemeric Unit (Cambel & Jarkovský, 1985; Hurai et al., 2008). In the

Tab. 9 Electron microprobe analyses of the Cu-S minerals covellite (Cv) and spionkopite (Spi) from the Brusno-Brzáčka occurrence. Atomic proportions of Cv are calculated on the basis of 6 cations and those of Spi on the basis of 19.5 cations; n. a. – not analysed.

an.	1	2	3	4	5	6	7	8	9	10	11
mineral	Cv	Cv	Cv	Cv	Cv	Cv	Cv	Cv	Cv	Spi	Spi
Ag	0.35	2.08	0.48	0.53	0.50	0.63	0.30	5.94	1.74	2.88	2.45
Cu	64.71	64.21	64.11	64.88	64.98	64.92	65.03	60.62	65.00	67.24	68.54
Zn	0.00	0.09	0.00	0.07	0.09	0.06	0.01	0.15	0.06	0.00	0.10
Hg	n. a.	n. a.	n. a.	n. a.	n. a.	n. a.	n. a.	n. a.	n. a.	n. a.	n. a.
Pb	n. a.	n. a.	n. a.	n. a.	n. a.	n. a.	n. a.	n. a.	n. a.	n. a.	n. a.
Bi	n. a.	n. a.	n. a.	0.23	0.18	0.19	0.12	0.08	0.25	0.54	0.43
S	33.60	32.00	34.30	33.11	33.90	33.48	33.05	32.65	32.53	27.19	27.18
Se	0.16	0.72	0.04	0.00	0.11	0.00	0.01	0.02	0.29	0.49	0.11
Σ wt. %	98.67	98.39	98.89	98.81	99.65	99.28	98.52	99.45	99.59	97.84	98.71
						atomic proportions					
Ag^{+}	0.019	0.112	0.026	0.028	0.027	0.034	0.016	0.327	0.093	0.479	0.402
Cu^{2+}	5.981	5.880	5.974	5.959	5.960	5.955	5.979	5.657	5.895	18.975	19.035
Zn^{2+}	0.000	0.008	0.000	0.006	0.008	0.006	0.001	0.014	0.005	0.000	0.028
Hg^{2+}	n. a.	n. a.	n. a.	n. a.	n. a.	n. a.	n. a.	n. a.	n. a.	n. a.	n. a.
Pb^{2+}	n. a.	n. a.	n. a.	n. a.	n. a.	n. a.	n. a.	n. a.	n. a.	n. a.	n. a.
Bi^{3+}	n. a.	n. a.	n. a.	0.006	0.005	0.005	0.003	0.002	0.007	0.046	0.036
Σ	6.000	6.000	6.000	6.000	6.000	6.000	6.000	6.000	6.000	19.500	19.500
S^{2-}	6.063	6.154	5.808	6.334	6.026	6.163	6.087	6.023	6.039	15.204	14.959
Se^{2-}	0.008	0.012	0.053	0.003	0.000	0.008	0.000	0.000	0.002	0.112	0.025
Σ	6.071	6.165	5.861	6.337	6.026	6.171	6.087	6.023	6.040	15.316	14.984

case of the Brzáčka occurrence, the carbonate period was not found. The reason thereof could be also total conversion of carbonates to Fe oxides. The overall very weak development of mineralization should be emphasized again.

The geological position of the occurrence at an interface between Upper Permian and Lower Triassic sedimentary rocks (Slavkay et al., 2004) as well as the nature of the hydrothermal mineralization clearly indicate its Paleoalpine age. The ore minerals were probably formed during mild dynamometamorphism, which is evidenced by the transformation of clastic sediments into sericitic phyllites, pressure lamellae, migration of mineral grain edges and newly formed grains in pre-existing **quartz I** and baryte. It is therefore a metamorphic-hydrothermal mineralization. Lexa et al. (2007) place this occurrence to the Paleoalpine, late orogenic metallogenetic stage of the Slovak part of the Carpathians development (90–70 Ma; Upper Cretaceous). The temperature conditions of Alpine metamorphism in the Northern Veporic did not exceed 350 °C, while the maximum temperatures were reached in the period between about 80–70 Ma (Plašienka, 2018; Majzlan et al., 2022 and citations therein). It can therefore be assumed that the studied hydrothermal mineralization at Brzáčka occurrence was formed after the peak of metamorphism during cooling of the system, perhaps in the Upper Cretaceous period.

5.2. Notes on the evolution of supergene zone

In contrast to the hydrothermal phase, the relationships among minerals formed in the **supergene phase** of mineralization are somewhat clearer. The Cu-S sulfides **covellite** and **spionkopite** formed in the first oxidation stage of preexisting sulfidic minerals. Oxidizing conditions began to prevail as the erosion cut progressed. Probably the oldest ***oxidation zone*** minerals are **goethite**, **pyromorphite** and **mimetite**. They were followed by the crystallization of **Ba-rich anglesite**, which overlaps in time with the precipitation of slightly younger **anglesite**. The formation of **baryte** partly overlaps with the deposition of anglesite, but in most cases it is clearly younger. Rare bismutite is probably the youngest oxidation mineral. A similar evolution of the supergene zone (sulfides → arsenates → sulfates → carbonates) was detected within the Cu-As-Pb-Zn mineralization at the Cap Garonne deposit in France (Poot et al., 2023). A more advanced stage of supergene alteration of galena (with practically the same association of supergene minerals), documented by the dissolution of cerussite and anglesite, is reported by Keim and Markl (2015). Direct replacement of galena by anglesite has been found in many cases, while the alteration of anglesite to other supergene phases (e.g. carbonates) is the result of a change in the chemical composition of supergene solutions accompanied by a decrease in the concentration of sulfate ions (Williams, 1990). Neglecting the extremely rare occurrence of bismutite, the absence of carbonates at the site therefore reflects a very low concentration of dissolved CO_3^{2-} ions in the supergene solutions. This is caused by the fact that the host rocks (Lower Triassic and Permian clastic sediments) have neither a carbonate matrix nor carbonate clasts.

The supergene zone at the Brzáčka occurrence is very weakly developed. Despite this, some mineral phases (bismutite, mimetite, pyromorphite), or interesting baryte-anglesite solid solution, which are still relatively rare for Slovakia, were found in the apparently weakly mineralized samples. Also noteworthy is the slightly increased bismuth content, the main carrier of which is galena (on average 0.015 *apfu* Bi), less Bi is present in tetrahedrite-(Zn) (0.017 *apfu* Bi in average). Due the supergene alteration, mainly of galena, bismuth enters to the secondary minerals, either as the major element (bismutite; ~1.57 *apfu* Bi), or as a minor element, e.g., in anglesite and Ba-rich anglesite (on average 0.040 *apfu* Bi), also in pyromorphite (~ 0.05 *apfu* Bi) and mimetite (~ 0.07 *apfu* Bi).

5.3. About bario-anglesite (Ba-rich anglesite)

Baryte-group minerals are defined by a general chemical formula AXO_4, in which the A position is occupied by divalent Ba, Sr, or Pb ions and the X position is occupied by S^{6+} or Cr^{6+} ions. Baryte is the most common member of the baryte group, the other three are anglesite ($PbSO_4$), celestine ($SrSO_4$) and hashemite ($BaCrO_4$). Thus, the difference in chemical composition is represented only by their metal cations. Strontium and lead, with their similar valences and ionic radii, easily replace Ba. Barium and strontium replace each other very easily, therefore baryte and celestine form a complete series of solid solutions with intermediate phases like barium-celestine, *"celestobarite"*, or *"baritocelestine"*. Baryte also forms a partial solid solution series with anglesite, with an intermediate phase known as *"plumbobarite"* (Klein & Philpotts, 2013; Johnson et al., 2017). In the past, Pb-rich baryte was also referred to as *"hokutolite"* or *"anglesobarite"*. Generally, it is a rare mineral phase, found in only a few occurrences in the world. It was first discovered in 1905 at locality Peitou (Hokuto; Chang 1961) Springs (Taiwan; mindat.org). In Japan, Pb-rich baryte was found at Tamagawa Hot Springs and Kawarge localities. In these sites, it crystallized from hyperacidic (pH <2), SO_4 – Cl geothermal waters, at a temperature around 60 °C (Takano et al., 1969; Yoshiike, 2003). Such Pb-rich baryte is also a bearer of certain amounts of Ra, as well as U and Th, therefore it is possible to search for it in places of natural occurrence also on the basis of increased radioactivity (Momoshima et al., 1997; Tomita et al., 2006; Chao et al., 2009). In addition, microcrystals of the baryte-anglesite solid solution of were found on heaps after mining activities, e.g. the Sandsloot mine site in South Africa (mindat.org/min-9160.html; Courtin-Nomade et al., 2008), Cínovec in Czech Republic (Pauliš et al., 1998) and in contaminated soils (Caboche et al., 2010).

In the literature, the completeness of the $PbSO_4$ – $BaSO_4$ solid solution is quite often discussed in terms of metastability, or the immiscibility of phases with a certain Pb/Ba ratio (Takano et al., 1969; Takiyama, 1967; Boström et al., 1967). Based on analytical data (Fig. 7 and the references therein), it is known that the natural Pb-rich baryte contains max. ~ 47 mol. % $PbSO_4$. On the contrary, it was possible to synthesize a complete $PbSO_4$ – $BaSO_4$ solid solution under laboratory conditions (Wang et al., 2002; Lee et al., 2005).

At the Brzáčka occurrence, we identified the baryte-anglesite solid solution (Ba-rich anglesite) with a Ba content from 0.002 *apfu* up to 0.51 *apfu* Ba. This mineral phase covers the field of immiscibility of the natural $PbSO_4$ - $BaSO_4$ solid solution (Fig. 7), but the Ba/Pb ratio practically does not enter to the baryte field. The Ba-rich anglesite was formed here under supergene conditions, from cold, probably slightly to moderately acidic near-surface solutions. In the locality, the average annual air temperature is 4–6 °C, the average annual temperature of the soil surface is 7–8 °C (Atlas of the landscape of Slovak Republic, online). The most amounts of Pb-rich baryte is formed mainly from hyperacidic and tempered solutions (60 °C), much less under supergene conditions (Takano et al., 1969; Yoshiike, 2003; Courtin-Nomade et al., 2008; Caboche et al., 2010). This fact indicates, that natural members of solid solution with Ba/(Ba+Pb) ratio in the range of 0.002–0.50 (corresponding to Ba-rich anglesite) can be preferentially formed from cold solutions, whereas members with Ba/(Ba+Pb) ranging 0.53–0.99 (i.e., corresponding to Pb-rich baryte) preferentially precipitate at higher temperatures.

Acknowledgements: This work was supported by the Ministry of Education, Slovak Republic VEGA-1/0563/22 project, as well as by the Slovak Research and Development Agency under the contract APVV-22-0092, and KEGA 033UMB-4/2021project. Analytical works were also financially supported by the Ministry of Culture of the Czech Republic (long-term project DKRVO 2024-2028/1.I.a; National Museum, 00023272) to Z.D. Authors thank to reviewers Juraj Majzlan and Jiří Sejkora, for detailed reviews and improvement of the manuscript.

References

Antalík M. & Káčer Š., 2005: Tektonická schéma slovenskej časti Západných Karpát. [Tectonic scheme of the Slovak part of the Western Carpathians]. http://www.mineraly.sk/files/lok/20_geolog_stavba_sr.htm, 13. 3. 2023. [in Slovak]

Biagioni C., George L. L., Cook N. J., Makovicky E., Moëlo Y., Pasero M., Sejkora J., Stanley C. J., Welch M. D. & Bosi F., 2020: The tetrahedrite group: Nomenclature and classification. American Mineralogist 105, 109–122.

Böstrom K., Frazer J. & Blankenburg J., 1967: Subsolidus phase relations and lattice constants in the system $BaSO_4$ –$SrSO_4$–$PbSO_4$. Arkive Min. Geol. 4, 477–485.

Caboche J., Debys S., Feidt C., Delalain P., Tack K. & Rychen G., 2010: Modelling Pb bioaccesibility in soils contaminated by mining and smelting activities. Journal of Environmental Science and Health, Part A Toxic/Hazardous Substances & Environmental Engineering 45, 10, 1264–1274.

Cambel B., Jarkovský J. (eds.), Faith L., Forgáč J., Hovorka D., Hrnčárová M., Hurný J., Ivan P., Karoli A., Kráľ J., Litavec J., Matula I., Mihalov J., Popreňák J., Rényi K., Rojkovič I., Rozložník L., Sasvári T., Savčenková L., Spišiak J., Šmejkal V., Turan J., Turanová L., Varček C., Žabka M. & Žukov, F., 1985: Rudňany ore field – geochemical-metallogenetic characteristic. Veda, Bratislava, 365. [in Slovak with English Summary]

Chang F. H., 1961: Genetic study of anglesobarite from Peitou, Taiwan. Acta Geol Taiwan 9, 7–17.

Chao J. H., Chuang C. Y., Yeh S. A. & Wu J. M., 2009: Relationship between radioactivity of radium and concentrations of barium and lead in hokutolite. Applied Radiation and Isotopes 67, 650–653.

Courtin-Nomade A., Soubrand-Colin M., Marcus M. A. & Fakra S. C. 2008: Evidence for the incorporation of lead into barite from waste rock pile materials. Environmental Science and Technology 42, 8, 2867–2872.

Ferenc Š., Bakos F., Demko R. & Koděra P., 2014: Siderite (Fe carbonate) and quartz-sulphidic mineralization occurrences near Lovinobaňa and Uderiná (Slovenské Rudohorie Mts.-Veporic Unit), Slovak Republic. Bulletin mineralogicko-petrologického oddělení Národního muzea v Praze, 22/1, 25–41. [in Slovak with English Abstract]

Ferenc Š, Vlasáč J, Mikuš T, Šimonová V. & Olšavský M., 2019: Ľubietová-Peklo - small occurrence of Cu^{-}(± Ag) ores hidden in the shadow of „copper giants" (Slovenské Rudohorie Mts., Veporic Unit, Western Carpathians). Bulletin mineralogicko-petrologického oddělení Národního muzea v Praze, 27/1, 46–62. [in Slovak with English Abstract]

Goble R. J., 1985: The relationship between crystal structure, bonding and cell dimensions in the copper sulfides. The Canadian Mineralogist 23, 61–76.

Hók J., Pelech O., Teťák F., Németh Z. & Nagy A., 2019: Outline of the geology of Slovakia (W. Carpathians). Mineralia Slovaca, 51, 31–60.

Hurai V., Lexa O., Schulmann K., Montigny R., Prochaska W., Frank W., Konečný P., Kráľ J., Thomas R. & Chovan M, 2008. Mobilization of ore fluids during Alpine metamorphism: evidence from hydrothermal veins in the Variscan basement of Western Carpathians, Slovakia. Geofluids 8, 181–207.

Hvožďara P., 1971: Štúdium zlatých mineralizácií niektorých jadrových pohorí Západných Karpát. [Study of the gold mineralization in some core mountains of the Western Carpathians]. Final report, archive of Geofond, Bratislava, 184. [in Slovak]

Hvožďara P., 1980: Prospekčné minerály tatroveporidného kryštalinika. [Prospective minerals of the Tatroveporide crystalline complex] Acta Geologica et Geographica Universitatis Comenianae, Geologica, Bratislava, 35, 5–43.

Johnson C. A., Piatak N. M. & Miller M. M., 2017: Chapter D of Critical Mineral Resources of the United States – Economic and Environmental Geology and Prospects for Future Supply. In: Schulz K. J., Deyoung J. H., Seal II R. R. & Bradley D. C. (Eds): Critical Mineral Resources of the United States – Economic and Environmental Geology and Prospects for Future Supply. U.S. Geological Survey, Reston, Virginia. 1–18.

Keim M. F. & Markl G., 2015: Weathering of galena: Mineralogical processes, hydrogeochemical fluid path modeling, and estimation of the growth rate of pyromorphite. American Mineralogist, 100, 1584–1594.

Klein C. & Philpotts A., 2013: Earth Materials – Introduction to Mineralogy and Petrology. New Yourk, Cambridge University Press, 536 p.

Koděra M., Andrusová-Vlčeková G., Belešová O., Briatková D., Dávidová Š., Fejdiová V., Hurai V., Chovan M., Nelišerová E. & Ženiš P., 1986: Topographic mineralogy of Slovakia I-III. Veda - vydavateľstvo SAV, Bratislava, 1590 p. [in Slovak with English Abstract]

Kováč M. & Plašienka D., 2003: Geologická stavba oblasti na styku Alpsko-karpatsko-panónskej sústavy a priľahlých svahov Českého masívu: vysokoškolské učebné texty. [Geological structure of the area at the junction of the Alpine-Carpathian-Pannonian system and the adjacent slopes of the Czech Massif]. Univerzita Komenského, 85 p. [in Slovak]

Lee J. S., Wang H. R., Izuka I. & Yu, S. C., 2005: Crystal structure and Raman spectral studies of $BaSO_4$–$PbSO_4$ solid solution. Zeitschrift für Kristallographie 220, 1, 1–9.

Lexa J., Bačo P., Hurai V., Chovan M., Koděra P., Petro M., Rojkovič I. & Tréger M., 2007: Explanations to metallogenetic map of the Slovakia, 1:500 000. ŠGÚDŠ, Bratislava, 178. [in Slovak with English Summary]

Maheľ M., Kamenický J., Fusán O. & Matějka A., 1967: Regionální geologie ČSSR, díl II – Západní Karpaty. [Ragional geology of the Czechoslovakia, part II – Western Carpathians]. Academia, nakl. ČSAV, Praha. 486 p. [in Czech]

Majzlan J., Mikuš T. & Milovský R., 2022: Small occurrences of Middle Triassic ore mineralizations in the Western Carpathians. Acta Geologica Slovaca 14, 2, 103–114.

Mazúr E. & Lukniš M., 1980: Regionálna geografická syntéza Slovenskej socialistickej republiky, súbor diagnostických a prognostických máp o krajine a životnom prostredí. Regionálne geomorfologické členenie, M 1: 500 000. [Regional geographic synthesis of the Slovak Socialist Republic, a set of diagnostic and prognostic maps about the country and the environment. Regional geomorphological division, M 1 : 500 000]. Bratislava, Geogr. Ústav SAV. [in Slovak]

Mazúr E. & Lukniš M., 1986: Geomorfologické členenie SSR a ČSSR. M 1 : 1 000 000. In: Hrnčiarová T. (Ed.): Atlas krajiny SR. [Geomorphological division of SSR and Czechoslovakia. M 1 : 1 000 000]. Bratislava: Ministerstvo životného prostredia Slovenskej republiky, 2002. [in Slovak]

Momoshima N., Nita J., Maeda Y., Sugihara S., Shinno I., Matsuoka N. & Huang C. V., 1997: Chemical composition and radioactivity in hokutolite (plumbian barite) collected at Peito Hot Spring, Taiwan. Journal of Environmental Radioactivity, 37, 1, 85–99.

Pauliš P., Novák F., Jansa J. & Scharmová M., 1998: Supergenní minerály Sn-W ložiska Cínovec v Krušných horách (Česká republika). Bulletin mineralogicko-petrologického oddělení Národního muzea v Praze 6, 83.

Pasero M., Kampf A. R., Ferraris C., Pekov I. V., Rakovan J. & White T. J., 2010: Nomenclature of the apatite supergroup minerals. Eur. J. Mineral. 22, 163–179.

Planderová E. & Vozárová A., 1982: Biostratigraphical correlation of the Late Paleozoic formation in the West Carpathians. In: Sassi F. P. (Ed.): Newsletter No 4, IGCP Project No 5., 67–71.

Plašienka D., 1999: Tectonochronology and paleotectonic evolution of the Central Western Carpathians during the Jurassic and Creatceous. Bratislava: Veda Publ., 127.

Plašienka D., 2018: Continuity and episodicity in the early Alpine tectonic evolution of the Western Carpathians: How large-scale processes are expressed by the orogenic architecture and rock record data. Tectonics, 37, 7, 2029–2079.

Plašienka D.,Grecula P., Putiš M., Kováč M. & Hovorka D., 1997: Evolution and structure of the Western Carpathians: an overview. In: Grecula P., Hovorka D., Putiš M. (Eds.): Geological evolution of the Western Carpathians. Mineralia Slovaca, Monograph, Bratislava, 1–24.

Polák M. (Ed.), Filo I., Havrila M., Bezák V., Kohút M., Kováč P., Vozár J., Mello J., Maglay J., Elečko M., Olšavský M., Pristaš J., Siman P., Buček S., Hók J., Rakús M., Lexa J., Šimon L., Buček S., Rakús M., Lexa J. & Šimon L., 2003a: Geologická mapa Starohorských vrchov, Čierťaže a severnej časti Zvolenskej kotliny, M 1 : 50 000. [Geological map of the Staré Hory Mts., Čierťaž and North part of the Zvolen basin, 1: 50 000]. MŽP SR – ŠGÚDŠ, Bratislava. [in Slovak]

Polák M. (Ed.), Filo I., Havrila M., Bezák V., Kohút M., Kováč P., Vozár J., Mello J., Maglay J., Elečko M., Vozárová A., Olšavský M., Siman P., Buček S., Siráňová Z., Hók J., Rakús M., Lexa J., Šimon L., Pristaš J., Kubeš P., Zakovič M., Liščák P., Žáková E., Boorová D. & Vaněková H., 2003b: Explanations to the geological map of the Staré Hory Mts., Čierťaž and North part of the Zvolen basin, 1: 50 000. ŠGÚDŠ, Bratislava, 218. [in Slovak with English Summary]

Poot J., Yans J., Gaëtan R., Buelens P. & Dekoninck A., 2023: Weathering processes associated to the formation of supergene Cu-As-Pb-Zn minerals at the Cap Garonne mine (France, Provence). Proceedings from 17th SGA Biennial Meeting, Zürich, 21–24.

Pouchou, J. L. & Pichoir, F., 1985: “PAP” (φρZ) procedure for improved quantitative microanalysis. In: Armstrong J. T. (Ed): Microbeam Analysis. San Francisco Press, 104–106.

Putiš M., 1992: Variscan and Alpidic nappe structures of the Western Carpathians crystalline basement. Geologica Carpathica (Bratislava) 23, 459–473.

Sasaki N. & Minato H., 1982: Relationship between lattice constants and strontium and calcium contents of hokutolite. Mineralogical Journal, 11, 2, 62–71.

Sasaki N. & Watanuki K., 1983: Variation in chemical composition of naturally occurring lead-bearing barite (hokutolite) having crystallized since 1953 at Tamagawa Hot Spring. Mineralogical Journal, 11, 6, 297–302.

Sasaki N., Yamashita A. & Watanuki K., 1992: The chemical composition of plumbian barite (hokutolite) precipitated from 1981 to 1990 at Tamagawa Hot Springs, Akita Prefecture, Japan. Mineralogical Journal, 16, 1, 49–59.

Siegel K., 1982: Structure of the vepor pluton (West Carpathians). Geological proceedings Geologica Carpathica, 33, 2, 171–175.

Slavkay M., Beňka J., Bezák V., Gargulák M., Hraško Ľ., Kováčik M., Petro M., Vozárová A., Hruškovič S., Knésl J., Knéslová A., Kusein M., Maťová V. & Tulis J., 2004: Mineral deposits of the Slovak Ore Mountains, vol. 2. GÚDŠ Bratislava. 286 p. [in Slovak with English Summary]

Slavkay M. & Petro M., 1993: Metallogenesis and ore formations of the Veporic Unit. Mineralia Slovaca 25, 313–317. [in Slovak with English Abstract]

Takano B., Yanagisawa M. & Watanuki K., 1969: Structure gap in $BaSO_4$–$PbSO_4$ solid solution series. Mineralogical Journal 6, 3, 159–171.

Takiyama K., 1967: Proceedings of the 16th Annual Meeting of the Japan Society for Analytical Chemistry. 2B04.

Tomita J., Sakaguchi A. & Yamamoto M., 2006: Hokutolite collected from riverbed at Peitou Hot Spring in Taiwan: With emphasis on radiochemical studies. Journal of Radioanalytical and Nuclear Chemistry, 270, 3, 567–574.

Vozárová A., 1979: Lithofacial characteristics of Permian in NW part of Veporicum. Západné Karpaty. Séria mineralógia, petrológia, geochémia, metalogenéza 6, 61–116. [in Slovak with English Summary]

Vozárová A., Rodionov N., Vozár J., Lepekhina E. & Šrinová K., 2016: U-Pb zircon ages from Permian volcanic rocks and tonalite of the Northern Veporicum (Western Carpathians). Journal of Geosciences 61, 221–237.

Vozárová A. & Vozár J., 1988: Late Paleozoic in West Carpathians, GÚDŠ Bratislava. 314 p.Wang H. R., Lee J. S. & Yu S. C., 2002: Synthesis of zoning-free $BaSO_4$–$PbSO_4$ solid solution and its structural characterizations. Zeitschrift für Kristallographie 217, 143–148.

Williams P. A., 1990: Oxide zone geochemistry. Ellis Horvood, Chichester, England. 286 p.

Yoshiike Y., 2003: Variation in the chemical composition of Obuki Spring, Tamagawa Hot Springs (1951–2000). Geochemical Journal 37, 6, 649–662.

Zoubek V., 1957: Hranice gemeríd a veporíd. [Borders of Gemeric Unit and Veporic Unit] Geologické Práce, Zošit 46, 38–50. [in Slovak]

Zoubek V., 1936: Poznámky o krystaliniku Západních Karpat. [Notes on the crystalline complex of the Western Carpathians]. Věstník Státního geologického ústavu Československé republiky 12, 207–239. https://www.mindat.org/min-9160.html, 30. 7. 2023. [in Czech]

Atlas krajiny SR. [Atlas of the landscape of Slovak Republic] https://app.sazp.sk/atlassr/, 27. 10. 2023

Mindat.org – Hokutolite. https://www.mindat.org/min-9160.html, 11. 8. 2023

Supp. Tab. S1 Spectral lines, crystals and standards used for WDS microanalyses.

EPMA Banská Bystrica				EPMA Praha			
element	line	crystal	standard	element	line	crystal	standard
Ca	Kα	PETL	Diopside	Ca	Kα	LPET	Wollastonite
Bi	Mα	PETH	Bi_2Se_3	Ca	Kα	LPET	Apatite
Bi	Lα	LIF	Bi_2Se_3	Bi	Mα	LPET	Bi
Sr	Lα	PETH	Celestine	Bi	Mß	LPET	Bi_2Se_3
Sr	Lß	TAP	Celestine	Sr	Lß	LPET	Celestine
Ba	Lα	PETL	Baryte	Ba	Lα	LPET	Baryte
Ba	Lα	LIF	Baryte	Ba	Lß	LLIF	Baryte
Fe	Kα	LIFH	Hematite	Fe	Kα	LLIF	Pyrite
Fe	Kα	LIFL	Pyrite	Fe	Kα	LLIF	Hematite
Fe	Kα	LIF	Olivine	Co	Kα	LLIF	Co
Co	Kα	LIFH	Co	Ni	Kα	LLIF	Ni
Ni	Kα	LIFH	Gersdorffite	F	Kα	LCP1	LiF
F	Kα	LDE1	Fluorite	Cd	Lα	LPET	CdTe
Cd	Lα	PETJ	CdTe	Cu	Kα	LLIF	Chalcopyrite
Cu	Kα	LIFH	Cuprite	Mn	Kα	LPET	Rhodonite
Cu	Kα	LIFH	Chalcopyrite	Mn	Kα	LLIF	Mn
Mn	Kα	LIFL	Rhodonite	Mg	Kα	LTAP	Diopside
Mg	Kα	TAP	Diopside	Zn	Kα	LLIF	ZnO
Zn	Kα	LIF	Sphalerite	Zn	Kα	LLIF	ZnS
Zn	Kα	LIF	Willemite	Hg	Lα	LLIF	HgTe
Zn	Kα	LIFH	Gahnite	Pb	Mα	LPET	Wulfenite
Hg	Mα	PETL	Cinnabar	Pb	Mα	LPET	Vanadinite
Pb	Mα	PETJ	Galena	Pb	Mα	LPET	PbS
Pb	Mß	PETL	Crocoite	Au	Mα	LPET	Au
Au	Mα	PETH	Au	Ag	Lα	LPET	Ag
Ag	Lα	PETL	Ag	Na	Kα	LTAP	Albite
Na	Kα	TAP	Albite	K	Kα	LPET	Sanidine
K	Kα	PETL	Orthoclase	Cl	Kα	LPET	Halite
Cl	Kα	PETL	Tugtupite	Al	Kα	LTAP	Sanidine
Al	Kα	TAP	Albite	S	Kα	LPET	Celestine
S	Kα	PETL	Baryte	S	Kα	LPET	Chalcopyrite
S	Kα	PETJ	Pyrite	P	Kα	LTAP	Apatite
P	Kα	PETL	Apatite	As	Lß	LTAP	Arsenopyrite
As	Lß	TAP	Arsenopyrite	As	Lß	LTAP	GaAs
As	Lß	TAP	GaAs	As	Lα	LTAP	Clinoclase
V	Kα	LIF	$ScVO_4$	As	Lß	LTAP	NiAs
Cr	Kα	LIF	Cr_2O_3	V	Kα	LLIF	Vanadinite
Sb	Lα	PETL	Stibnite	Sb	Lα	LPET	Sb_2S_3
Sb	Lα	PETH	Stibnite	Si	Kα	TAP	Wollastonite
Si	Kα	TAP	Plagioclase	Si	Kα	TAP	Sanidine-PS39B
Si	Kα	TAP	Orthoclase	Se	Lß	LTAP	PbSe
Zr	Lα	PETL	ZrO_2	Te	Lα	LPET	PbTe
Zr	Lß	PETL	ZrO_2	Ge	Lα	LTAP	Ge
Se	Lß	TAP	Bi_2Se_3	Ga	Lα	LTAP	GaAs
Te	Lα	PETL	CdTe	I	Lß	LPET	Tl(Br, I)
Ti	Kα	LIF	Rutile	Sn	Lα	LPET	Sn
				Br	Lα	LTAP	Tl(Br, I)